Molecular Biology of the Cell
Vol. 8, 729–753, April 1997

Aip3p/Bud6p, a Yeast Actin-interacting Protein That Is Involved in Morphogenesis and the Selection of Bipolar Budding Sites

David C. Amberg,*†‡ Joseph E. Zahner,†§ Jon W. Mulholland,* John R. Pringle,§ and David Botstein*

*Department of Genetics, Stanford University School of Medicine, Stanford, California 94305-5120; and §Department of Biology, University of North Carolina, Chapel Hill, North Carolina 27599-3280

Submitted September 13, 1996; Accepted December 23, 1996
Monitoring Editor: Randy Schekman

A search for *Saccharomyces cerevisiae* proteins that interact with actin in the two-hybrid system and a screen for mutants that affect the bipolar budding pattern identified the same gene, *AIP3/BUD6*. This gene is not essential for mitotic growth but is necessary for normal morphogenesis. *MAT***a**/α daughter cells lacking Aip3p place their first buds normally at their distal poles but choose random sites for budding in subsequent cell cycles. This suggests that actin and associated proteins are involved in placing the bipolar positional marker at the division site but not at the distal tip of the daughter cell. In addition, although *aip3* mutant cells are not obviously defective in the initial polarization of the cytoskeleton at the time of bud emergence, they appear to lose cytoskeletal polarity as the bud enlarges, resulting in the formation of cells that are larger and rounder than normal. *aip3* mutant cells also show inefficient nuclear migration and nuclear division, defects in the organization of the secretory system, and abnormal septation, all defects that presumably reflect the involvement of Aip3p in the organization and/or function of the actin cytoskeleton. The sequence of Aip3p is novel but contains a predicted coiled-coil domain near its C terminus that may mediate the observed homo-oligomerization of the protein. Aip3p shows a distinctive localization pattern that correlates well with its likely sites of action: it appears at the presumptive bud site prior to bud emergence, remains near the tips of small buds, and forms a ring (or pair of rings) in the mother-bud neck that is detectable early in the cell cycle but becomes more prominent prior to cytokinesis. Surprisingly, the localization of Aip3p does not appear to require either polarized actin or the septin proteins of the neck filaments.

INTRODUCTION

The yeast *Saccharomyces cerevisiae* reproduces by budding, a process that involves a highly polarized expansion of the cell surface. Buds are formed at nonrandom sites, and their polarized growth depends on an underlying polarization of the actin cytoskeleton (Pringle *et al.*, 1995; Drubin and Nelson, 1996). The actin cytoskeleton of yeast is organized into cortical patches of filamentous actin and bundles of actin filaments (called actin cables) that extend along the long axis of budding cells. During the cell cycle, actin cortical patches first appear at the incipient bud site ~15 min before bud emergence (Kilmartin and Adams, 1984; Ford and Pringle, 1991; Snyder *et al.*, 1991). In small buds, the cortical patches are concentrated at the tip of the bud; later, the patches redistribute throughout the bud and eventually relocalize to the mother-bud neck just prior to and during cell division (Adams and Pringle, 1984; Kilmartin and Adams, 1984; Lew

† These authors contributed equally to this work.
‡ Corresponding author and present address: Department of Biochemistry and Molecular Biology, State University of New York Health Science Center at Syracuse, Weiskotten Hall #4283, 750 East Adams Street, Syracuse, NY 13210.

and Reed, 1993), suggesting that actin also has a role in cytokinesis.

The strongest evidence concerning the functional role of actin in various cellular processes derives from the behavior of actin mutants. Many mutations have been isolated in the single gene (*ACT1*) of *S. cerevisiae* that encodes conventional actin. The phenotypes of these mutants (and mutants of actin-binding proteins as well) have indicated that the actin cytoskeleton is involved in polarized secretion and cell surface growth, cell shape determination, endocytosis, mitochondrial distribution, nuclear migration, and cytokinesis (Drubin *et al.*, 1993; Kübler and Riezman, 1993; Bénédetti *et al.*, 1994; Bretscher *et al.*, 1994; Welch *et al.*, 1994). A particularly useful set of *act1* mutations was derived by clustered charged-to-alanine scanning mutagenesis (Wertman *et al.*, 1992); these mutations collectively alter much of the surface of the actin molecule as seen in the three-dimensional structure. Drubin *et al.* (1993) have studied this set of mutations and identified, among other things, alleles that affect both cell morphology and cytokinesis.

The exact role of actin in cytokinesis in yeast is uncertain, although it is quite clear that actin is intimately involved in cytokinesis in other cell types (for review, Fishkind and Wang, 1995). In yeast, actin could be involved in a contractile ring mechanism like that in animal cells, in the localized formation of septal cell wall, or both. Other proteins involved in cytokinesis in *S. cerevisiae* are the septins encoded by the *CDC3*, *CDC10*, *CDC11*, and *CDC12* genes (for review, Longtine *et al.*, 1996). Mutants defective in these genes continue to bud and divide their nuclei but never complete cytokinesis (Hartwell, 1971; Adams and Pringle, 1984). Cdc3p, Cdc11p, and Cdc12p have regions in their C termini that are predicted to form coiled coils and are believed to assemble into the 10-nm filaments observed in the neck region of budded cells (Byers and Goetsch, 1976a,b; Byers, 1981; Longtine *et al.*, 1996). The relationship between septin function and actin function in cytokinesis is not known in any system, and to date no protein that interacts directly with actin has been shown to be required for cytokinesis in *S. cerevisiae*.

Actin may also be involved in the mechanisms of bud-site selection. *S. cerevisiae* cells select bud sites (and hence their division planes) in either of two nonrandom patterns. **a** or α cells (e.g., normal haploids) typically bud adjacent to the immediately preceding division site (see Chant and Pringle, 1995 and references cited therein). This "axial" pattern appears to depend on a transient signal that marks the division site just long enough to direct selection of the bud site in the next cell cycle (Chant and Pringle, 1995); this signal appears to involve the products of the *BUD3* and *BUD4* genes, which localize to the mother-bud neck (and hence to the division site) in a septin-dependent manner (Chant *et al.*, 1995; Sanders and Herskowitz, 1996). In contrast, **a**/α cells bud in a "bipolar" pattern, in which either pole of the cell can be utilized for budding in any cell cycle (Chant and Pringle, 1995). The bipolar pattern appears to depend on persistent or permanent cortical markers that are deposited at the division site on both mother and daughter cells and at the distal tip of the daughter cell in each cell cycle (Chant and Pringle, 1995). Bud3p and Bud4p are not involved in bipolar budding (Chant and Herskowitz, 1991; Chant *et al.*, 1995; Sanders and Herskowitz, 1996), and the postulated cortical marker proteins remain to be identified. However, a genetic screen designed to identify these marker proteins (or proteins involved in their localization or recognition) has recently identified several candidate genes including *BUD6*, mutations in which randomize the budding of **a**/α cells but have no effect on the axial budding of **a** or α cells (Zahner *et al.*, 1996).

In addition, several lines of evidence now suggest that the actin cytoskeleton may be directly involved in the localization or recognition of the bipolar marker proteins. First, mutations in *ACT1* and in the genes for several known actin-interacting proteins have been found to randomize the budding of **a**/α cells without affecting the axial budding of **a** or α cells (Drubin *et al.*, 1993; Yang *et al.*, 1997). Second, mutations in *RVS161*, *RVS167*, and at least two interacting genes appear to affect the organization of the actin cytoskeleton and to disrupt the bipolar (but not the axial) budding pattern (Bauer *et al.*, 1993; Durrens *et al.*, 1995; Sivadon *et al.*, 1995).

Full understanding of the roles of actin in cytokinesis, bud site selection, and other processes will depend on identifying and characterizing all of the actin-binding proteins and other components of the actin cytoskeleton. A number of approaches have been used to identify such proteins in *S. cerevisiae*. In our last count, genetic methods had identified >50 genes whose products bind to, affect, or are affected by the actin cytoskeleton (Botstein, Amberg, Huffaker, Mulholland, Adams, Drubin, and Stearns, unpublished results). Yeast has been found to contain members of most of the classes of known actin-binding proteins including five myosins (Johnston *et al.*, 1991; Sweeney *et al.*, 1991; Haarer *et al.*, 1994; Goodson and Spudich, 1995; Goodson *et al.*, 1996), two tropomyosins (Liu and Bretscher, 1989; Drees *et al.*, 1995), a fimbrin class bundling protein (Adams *et al.*, 1991), capping protein (Amatruda and Cooper, 1992), profilin (Magdolen *et al.*, 1988), a cofilin filament-severing protein (Iida *et al.*, 1993; Moon *et al.*, 1993), and TCP-1 class chaperones (Ursic and Culbertson, 1991; Chen *et al.*, 1994; Miklos *et al.*, 1994; Vinh and Drubin, 1994). An important aspect of these investigations involves determining which proteins interact physically with actin and where on the actin structure they bind. At the simplest level, this information can help determine whether the ligand pro-

tein binds to monomers or to filaments. Both biochemical and genetic methods have been used to identify the Sac6p (fimbrin) binding site on actin (Holtzman *et al.*, 1994; Honts *et al.*, 1994), but in general yeast has not yet been exploited extensively for structure/function studies of actin.

One approach to the identification of interacting proteins is the two-hybrid system, which measures the ability of two proteins, separately fused to the two halves of the Gal4p transcriptional activator, to reconstitute full Gal4p activity via protein-protein interactions in vivo (Fields and Song, 1989). We have used this system to identify proteins capable of interacting with yeast actin and then examined the ability of these ligands to interact with 35 clustered charged-to-alanine mutants of actin (Amberg *et al.*, 1995a). Those mutations that disrupt the interaction between actin and a particular ligand can help describe where the ligand binds on the surface of the actin molecule. This approach identified some well known actin-binding proteins as well as three new actin-interacting proteins including the product of the *AIP3* gene. We report herein that *AIP3* is identical to *BUD6*, identified in studies of bipolar budding (see above). The localization of Aip3p/Bud6p and the phenotypes of cells lacking this protein suggest that it mediates actin's involvement in morphogenesis, nuclear migration, cytokinesis, and bud-site selection.

MATERIALS AND METHODS

Yeast Strains, Media, and Genetic and Microbiological Methods

Yeast strains are listed in Table 1. DBY5650 and DBY5651 were provided by S. Elledge (Baylor College of Medicine) and are also known as Y187 and Y190, respectively. DBY6924 and DBY6925 were provided by F. Winston (Harvard Medical School) and are also known as FY23 and FY86, respectively. DBY6525 was formed by mating DBY6924 to DBY6925. YEF473 was described previously (Bi and Pringle, 1996); YEF473B is a segregant from YEF473. YJZ233 was derived by mating two segregants from a cross of YJZ196 (Zahner *et al.*, 1996) to 1241–2D (Chant and Herskowitz, 1991). YJZ383 was derived by several crosses from the original *cdc12–6* mutant (Adams and Pringle, 1984). Other strains are described below.

Standard methods were used for growth, sporulation, and genetic analysis of yeast (Rose *et al.*, 1989). YM-P rich medium was as described previously (Lillie and Pringle, 1980). Plates for the two-hybrid analysis were made by supplementing standard synthetic (SD) medium with 10 μg/ml adenine and 25, 50, or 100 mM 3-amino-1,2,4-triazole (Sigma, St. Louis, MO).

Viability was estimated by counting the cells in exponentially growing cultures with a hemocytometer, plating cells on three YPD plates (100 cells/plate), incubating the plates at 30°C, and then determining the mean and SD of colony-forming units from these three plates.

DNA Manipulations and Plasmid Constructions

Standard methods of DNA manipulation (Sambrook *et al.*, 1989) were used except where noted. Yeast transformations were performed using electroporation (Becker and Guarente, 1991) or the lithium acetate method (Ito *et al.*, 1983). Double-stranded dideoxynucleotide sequencing was performed with the Sequenase reagent kit from United States Biochemicals (Cleveland, OH) according to the manufacturer's instructions. Primers 2-H1 (TGATGAAGATACCCCACC) and 2-H4 (GCGACCTCATGCTATACC) were used to sequence into the 5′ and 3′ ends, respectively, of the two-hybrid library inserts. To sequence *BUD6*, the 3.3-kb *Hin*dIII fragment from plasmid YCp111/H3.3 (see RESULTS) was subcloned into pBluescript KS+ and sequenced by primer walking starting with the M13 primers. Both strands were completely sequenced. DNA and protein sequence databases were searched with the National Center for Biotechnology Information BLAST E-mail server (Altschul *et al.*, 1990).

Table 1. *Saccharomyces cerevisiae* strains

Name	Genotype
DBY5650	α *gal4 gal80 his3 trp1-901 ade2-101 ura3-52 leu2-3,112 GAL → lacZ*
DBY5651	**a** *gal4 gal80 his3 trp1-901 ade2-101 ura3-52 leu2-3,112 URA3::GAL → lacZ LYS2::GAL → HIS3 cyh^r*
DBY6525	**a**/α *ura3-52/ura3-52 leu2-Δ1/leu2-Δ1 trp1-Δ63/TRP1 HIS3/his3-Δ200*
DBY6924	**a** *ura3-52 leu2-Δ1 trp1-Δ63*
DBY6925	α *ura3-52 leu2-Δ1 his3-Δ200*
DBY6936	**a**/α *ura3-52/ura3-52 leu2-Δ1/leu2-Δ1 trp1-Δ63/TRP1 HIS3/his3-Δ200 aip3-Δ1::URA3/AIP3*
DBY6937	**a** *ura3-52 leu2-Δ1 trp1-Δ63 aip3-Δ1::URA3*
DBY6938	α *ura3-52 leu2-Δ1 his3-Δ200 aip3-Δ1::URA3*
DBY6939	**a**/α *ura3-52/ura3-52 leu2-Δ1/leu2-Δ1 trp1-Δ63/TRP1 HIS3/his3-Δ200 aip3-Δ1::URA3/aip3-Δ1::URA3*
DBY7262	**a** *ura3-52 leu2-Δ1 trp1-Δ63 his3-Δ200 aip3-Δ1::URA3*
DBY7261	**a**/α *ura3-52/ura3-52 leu2-Δ1/leu2-Δ1 trp1-Δ63/TRP1 his3-Δ200/his3-Δ200 aip3-Δ2::HIS3/AIP3*
DBY7055	**a** *ura3-52 leu2-Δ1 trp1-Δ63 his3-Δ200 aip3-Δ2::HIS3*
DBY7056	α *ura3-52 leu2-Δ1 trp1-Δ63 his3-Δ200 aip3-Δ2::HIS3*
DBY7057	**a**/α *ura3-52/ura3-52 leu2-Δ1/leu2-Δ1 trp1-Δ63/trp1-Δ63 his3-Δ200/his3-Δ200 aip3-Δ2::HIS3/aip3-Δ2::HIS3*
YEF473	**a**/α *trp1-Δ63/trp1-Δ63 leu2-Δ1/leu2-Δ1 ura3-52/ura3-52 his3-Δ200/his3-Δ200 lys2-801/lys2-801*
YEF473B	α *trp1-Δ63 leu2-Δ1 ura3-52 his3-Δ200 lys2-801*
YJZ233	**a**/α *his4/his4 leu2/leu2 trp1/trp1 ura3/ura3 bud3::TRP1/bud3::TRP1 bud6-1/bud6-1*
YJZ356	α *trp1-Δ63 leu2-Δ1 ura3-52 his3-Δ200 lys2-801 aip3-Δ3::TRP1*
YJZ358	**a**/α *trp1-Δ63/trp1-Δ63 leu2-Δ1/leu2-Δ1 ura3-52/ura3-52 his3-Δ200/his3-Δ200 lys2-801/lys2-801 aip3-Δ3::TRP1/aip3-Δ3::TRP1*
YJZ383	**a**/α *trp1-Δ63/trp1-Δ63 leu2-Δ1/leu2-Δ1 ura3-52/ura3-52 his3-Δ200/his3-Δ200 cdc12-6/cdc12-6*

DNA fragments were radiolabeled by the random-primer method (Feinberg and Vogelstein, 1983). Isolated DNAs were physically mapped by hybridization to a set of ordered λ clones (American Type Culture Collection, Rockville, MD) that collectively encode the yeast genome (Riles *et al.*, 1993).

A *Bgl*II fragment from the *AIP3* cDNA clone pRB2186 (see RESULTS) was used to identify genomic clones carrying the full-length *AIP3* gene by using a standard colony hybridization procedure (Sambrook *et al.*, 1989). Briefly, *Escherichia coli* cells containing a *S. cerevisiae* genomic DNA library in YCp50-LEU2 (gift from F. Spencer and P. Hieter, Johns Hopkins School of Medicine) were plated, and 10,000 colonies were lifted onto nitrocellulose and probed with the *AIP3* probe. Positive clone pRB2246 was identified by polymerase chain reaction (PCR) using primers corresponding to sequences at the ends of the *AIP3* two-hybrid cDNA clones (primer 210, 5′-GCTCCAAACG-CATCTGAT-3′; primer 209, 5′-GGAAATTCAACACTTGCA-3′).

BUD6 was cloned by transforming a *bud6* mutant with the same genomic library. Transformants were stained with Calcofluor to visualize bud scars and examined for reversion from random to bipolar budding pattern as described (Zahner *et al.*, 1996). For further analysis, a 3.3-kb *Hin*dIII fragment that proved to contain the full-length *BUD6/AIP3* gene (see RESULTS) was subcloned into the low copy number *LEU2*-containing shuttle vector YCplac111 (Gietz and Sugino, 1988) and the high copy number *URA3*-containing shuttle vector YEp352 (Hill *et al.*, 1986), creating plasmids YCp111/H3.3 and YEp352/H3.3, respectively.

The method of two-hybrid analysis and construction of the actin-Gal4p DNA-binding domain (DBD) bait construct pRB1516 and its alanine-scan derivatives were described previously (Amberg *et al.*, 1995a). Plasmids pRB2188 and pRB2189 were constructed by excising the *AIP3*-bearing *Bgl*II fragment from plasmid pRB2187 (see Figure 1; the *Bgl*II sites are in the plasmid polylinker) and cloning it into the *Bam*HI site of plasmid pRB1508 (Amberg *et al.*, 1995a) such that the *AIP3* open reading frame (ORF) was fused in-frame to sequences encoding the Gal4p DBD. Plasmids pRB1504 (also known as pSE1111), pRB1505 (also known as pSE1112), and pRB2146 encode fusions to the Gal4p activation domain (AD) (pRB1504 and pRB2146) or Gal4p DBD (pRB1505) of Snf4p, Snf1p, and actin, respectively (S. Elledge, personal communication; Amberg *et al.*, 1995a).

To construct the GFP-Aip3p fusion, the entire *AIP3* ORF was amplified by PCR using Vent polymerase (New England Biolabs, Boston, MA) according to standard protocols with genomic clone pRB2246 (see above) as template and primers of sequence 5′-GGC-CAGATCTATGAAGATGGCCGTGGAT-3′ and 5′-GGCCGCTAG-CAGTAAACCCCGGCCCAAA-3′. The resulting product was digested with *Bgl*II and *Nhe*I [sites (underlined) included in the primers] and cloned into pRB2138 (Doyle and Botstein, 1996) that had been digested with *Bam*HI and *Xba*I. The resulting plasmid,

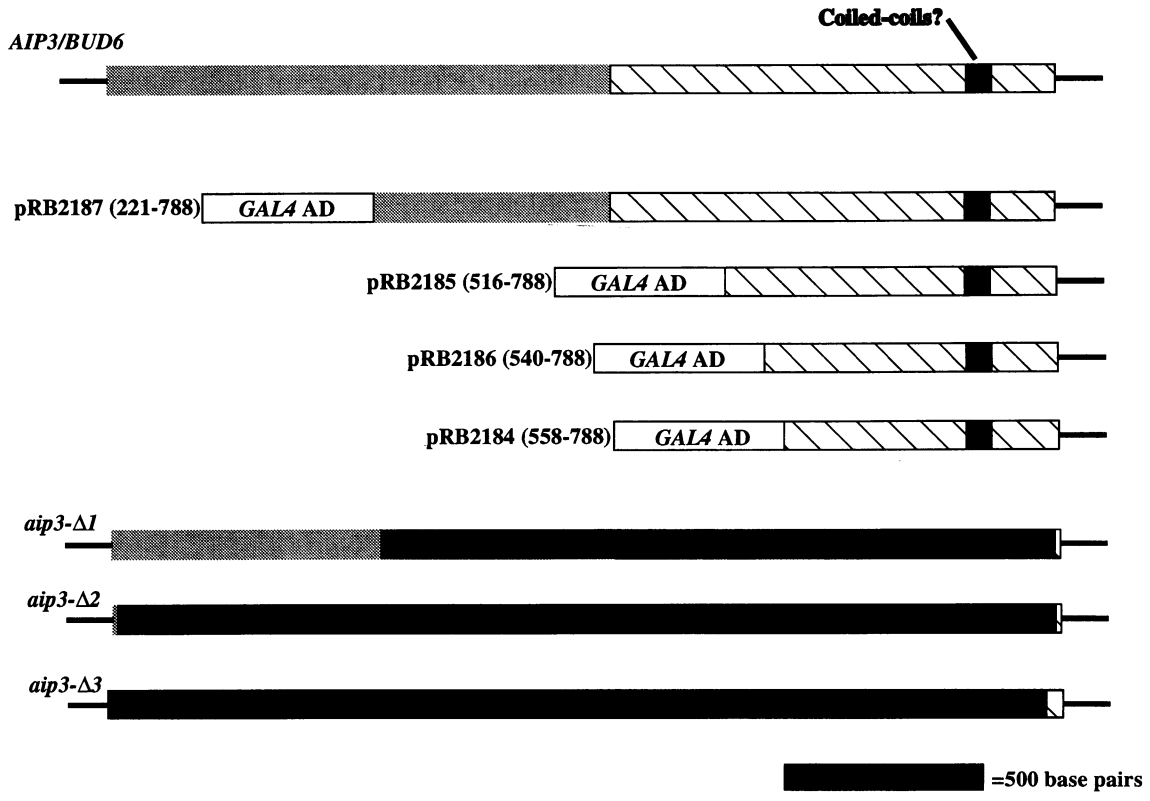

Figure 1. Sequence organization of *AIP3/BUD6*, two-hybrid cDNA clones, and deletion alleles. The organization of the *AIP3/BUD6* gene is shown at the top. The lightly shaded region is unique in sequence, the cross-hatched region is weakly homologous to many coiled coil-containing proteins, and the darkly shaded region is predicted by the Coils program (Lupas *et al.*, 1991) to form a coiled coil structure. The four Aip3p-encoding cDNA clones isolated from the two-hybrid screen are shown in the middle, and the organization of the deletion alleles is displayed at the bottom. The solid regions correspond to the sequences absent in the deletion alleles. The sequences determined for the full-length *BUD6* clone and for chromosome XII ORF YLR319C are available through GenBank (accession numbers L38903 and U20618, respectively) or the *Saccharomyces* Genome Database (http://genome-www.stanford.edu). There are a number of minor sequence differences (presumably polymorphisms) between the independently determined sequences.

pRB2190, encodes a fusion of GFP to the N terminus of Aip3p under the control of the actin promoter and terminator. Two additional independent isolates of this construct were also made and gave the same results as did pRB2190 when transformed into yeast.

Construction of AIP3 Disruption Alleles

Two deletion alleles of *AIP3* (*aip3-Δ1::URA3* and *aip3-Δ2::HIS3*) were constructed by double-fusion PCR (Amberg *et al.*, 1995b). The primers for the construction of disruption *aip3-Δ1* were A (primer 210; see above), B (5′-GTCGTGACTGGGAAAACCCTGGCGCGGTTTCCTCTAGATGCA-3′), C (5′-TCCTGTGTGAAATTGTTATCCGCTGGATAAGAAAGCAGAAGG-3′), and D (primer 209; see above). The primers for the construction of *aip3-Δ2* were A (5′-CTGTGATCTGCTTGCTTC-3′), B (5′-GTCGTGACTGGGAAAACCCTGGCGATC CACGGCCATCTTCAT-3′), C (5′-TCCTGTGTGAAATTGTTATCCGCTGGGCCGG GGTTTACTTAA-3′), and D (5′-CACCGTTCTCATGCAAATTGA-3′). The *URA3* and *HIS3* markers were amplified by using plasmids pJJ242 and pJJ215 (Jones and Prakash, 1990), respectively, as templates and the M13 "forward" and "reverse" sequencing primers. *AIP3* sequences were amplified from genomic clone pRB2246 (see above). The *aip3-Δ1::URA3* disruption cassette produced by double-fusion PCR was then introduced into strain DBY6525 to disrupt *AIP3*. To confirm this integration, colony PCR was performed by placing a small transformed yeast colony in 50 μl containing 20 mM Tris (pH 8.3), 1.5 mM $MgCl_2$, 25 mM KCl, 0.05% Tween 20, each primer at 500 nM, all four deoxynucleotide triphosphates (each at 200 μM), 100 μg/ml acetylated bovine serum albumin (New England Biolabs), and 1 μl of *Taq* polymerase (5 U, Life Technologies, Gaithersburg, MD). Primers A and D used for the *aip3-Δ1::URA3* disruption were used in the colony PCRs. These reactions were first heated to 94°C for 4 min and then subjected to 35 cycles of 94°C for 1 min, 55°C for 1 min, and 72°C for 3 min. Extensions were continued at 72°C for another 20 min. In this way, strain DBY6936 was confirmed to be heterozygous for the *aip3-Δ1::URA3* allele. An *aip3-Δ1::URA3* segregant from DBY6936 was mated to DBY6925, and the *aip3-Δ2::HIS3* disruption cassette produced by double-fusion PCR was introduced into the resulting diploid. His^+ transformants were screened for loss of the Ura^+ phenotype, and strain DBY7261 was confirmed to be heterozygous for the *aip3-Δ2::HIS3* allele by colony PCR. Strains DBY6937, DBY6938, and DBY6939 were derived from DBY6936, and strains DBY7055, DBY7056, and DBY7057 were derived from DBY7261, using standard genetic methods.

A third *AIP3* deletion allele (*aip3-Δ3::TRP1*) was constructed using the single-step PCR method (Baudin *et al.*, 1993). Primers 5′-CCAAATTGGTGTAGTAATCCTCGTATTATTTTAAAATTAGGTACAATCTTGATCCGGACC-3′ and 5′-GCTCTCAAATTTGCTTCATCCTTCTGCTTTCTTATCCTTTCTCCTTACGCATCTGTGCGG-3′ were used in a Vent polymerase PCR with plasmid pRS304 (Sikorski and Hieter, 1989) as template to generate a *TRP1* gene flanked by 40-mers corresponding to sequences immediately upstream of the *AIP3* start codon and 20 codons upstream of the stop codon. Trp^+ transformants of strain YEF473 were isolated, and their DNA was digested with *Hin*dIII. Southern blots were probed with a ^{32}P-labeled 600-bp *Sca*I-*Hin*dIII fragment of the 3′-flanking region of *AIP3*. Transformants yielding both 3.3-kb (derived from the wild-type allele) and 955-bp (derived from the disruption allele) fragments were presumed to have the genotype *AIP3/aip3-Δ3::TRP1*. Sporulation and tetrad analysis of such a strain showed a 2:2 segregation of Trp^+:Trp^-. Southern blot analysis demonstrated that all Trp^+ segregants carried the *aip3-Δ3::TRP1* allele. Strain YJZ356 (Table 1) is one such segregant; strain YJZ358 was obtained by mating two such segregants.

Generation of Antibodies to Aip3p

A 1.2-kb fragment of *AIP3* (codons 358–768) with an *Xba*I site at the 5′ end and a *Hin*dIII site at the 3′ end was amplified by PCR using Vent polymerase and primers 5′-GCTCTAGAATGAATGGAACTTGTCC-3′ and 5′-CCAAGCTTTTCTACTTCTTCAAAGCCTCC-3′. The template was the genomic 3.3-kb *Hin*dIII fragment containing the entire *AIP3* ORF from plasmid YCp111/H3.3 cloned into pBluescript KS+. The PCR product was digested with *Xba*I and *Hin*dIII, cloned into the corresponding sites of vector pMAL-c2 (New England Biolabs), and transformed into *E. coli* DH5α. DH5α cells containing the desired plasmid (as confirmed by sequencing across the junctions) were grown at 37°C to an OD_{600} of 0.6, then induced with 0.3 mM isopropyl-1-thio-β-D-galactopyranoside for 4 h to express the maltose-binding protein (MBP)-Aip3p fusion protein. Cells from 1 l of culture were pelleted, resuspended in 50 ml of column buffer (20 mM Tris-Cl, pH 7.0, 0.2 M NaCl, 1 mM EDTA), frozen on dry ice, thawed at room temperature, and sonicated for 30 s on ice. Cell debris was pelleted, and the clear supernatant was applied to a 20-ml amylose-agarose column (New England Biolabs) as described (Ausubel *et al.*, 1989). The column was first washed with 120 ml of column buffer and then with column buffer containing 10 mM maltose, and protein samples were analyzed with SDS-PAGE (Laemmli, 1970). The peak fraction contained predominantly a protein of ~78 kDa, the expected size for the MBP-Aip3p fusion protein.

The MBP-Aip3p fusion protein was used to raise a polyclonal rabbit antiserum according to standard procedures (Cocalico Biologicals, Reamstown, PA). Antisera were tested by Western blot analysis against the Aip3p fragment released from purified MBP-Aip3p by digestion with factor Xa protease (New England Biolabs) and adsorbed with amylose-agarose resin to remove the MBP fragment. Serum obtained after the fifth booster injection was affinity purified against the Aip3p fragment bound to N-Hydrozysuccinidnide (NHS)-activated Sepharose (Pharmacia Biotech, Piscataway, NJ). To purify the antibodies further by removing antibodies that bound to antigens other than Aip3p, the affinity-purified antibodies were then adsorbed repeatedly against cells of strain YJZ358 (*aip3-Δ3/aip3-Δ3*) that had been prepared as if for immunofluorescence with standard procedures (Pringle *et al.*, 1989) using yeast lytic enzyme (ICN, Costa Mesa, CA; catalogue number 152270) for digestion of cell walls. The purified antibodies were then concentrated using a Centricon-3 filter (Amicon, Danvers, MA) and bovine serum albumin was added to 0.1%.

Protein Analysis

For analysis of yeast proteins by Western blotting, cells from 5 ml of liquid culture in the mid-exponential phase (OD_{600} = 1) at 30°C were pelleted and resuspended in 500 μl of Laemmli sample buffer (Laemmli, 1970) at 100°C and incubated at 100°C for 5 min. After electrophoresis of 20-μl samples on a 10% SDS-polyacrylamide gel, proteins were transferred electrophoretically to an Immobilon-P polyvinylidene difluoride membrane (Millipore, Bedford, MA) in low-salt transfer buffer containing 20% methanol (Towbin *et al.*, 1979). Blots were stained with Coomassie blue to verify that the lanes contained equivalent amounts of protein and then destained with methanol. After blocking in TBST (10 mM Tris-Cl, pH 8.0, 150 mM NaCl, 0.05% Nonidet P-40) containing 5% nonfat dry milk, blots were incubated for 1 h at room temperature in purified anti-Aip3p antibodies diluted 1:1000 in TBST containing 0.1% bovine serum albumin and then washed three times (5 min per wash) in TBST. Blots were then probed with an alkaline phosphatase-conjugated goat anti-rabbit IgG secondary antibody (Jackson Immunoresearch, West Grove, PA) diluted 1:1000 in TBST containing 0.1% bovine serum albumin, washed three times in TBST, and developed with 5-bromo-4-chloro-3-indolyl phosphate and nitroblue tetrazolium as substrates as described previously (Harlow and Lane, 1988).

Light Microscopy

Overall cell morphologies were determined by differential interference contrast (DIC) microscopy. Staining of cell-wall chitin with Calcofluor, of nuclear DNA with 4,6-diamidino-2-phenylindole

(DAPI) or bisbenzimide (Sigma) and of filamentous (F) actin with rhodamine-phalloidin (Molecular Probes, Eugene, OR) were as described previously (Pringle *et al.*, 1989). Immunofluorescence localization of tubulin and Cdc11p was performed using standard protocols (Pringle *et al.*, 1989); for anti-tubulin immunofluorescence, fixation with 3.7% formaldehyde was followed by methanol/acetone treatment. YOL1/34 rat monoclonal antitubulin antibody (Accurate Chemical & Scientific, Westbury, NY) was used at a 1:100 dilution. Affinity-purified anti-Cdc11p (Ford and Pringle, 1991) was used at a 1:20 dilution. Rhodamine-conjugated goat anti-rabbit IgG (Jackson Immunoresearch) and fluorescein isothiocyanate-conjugated goat anti-rat IgG (Organon Teknika, Durham, NC) were used at 1:200 and 1:1000 dilutions, respectively. Cells were examined and photographed on a Zeiss Axioskop fitted with a Plan-Neofluar 100×/0.7–1.4 numerical aperture objective using hypersensitized Kodak Technical Pan 2415 film (Lumicon, Livermore, CA) or on a Nikon Microphot SA microscope using an Apo 60×/1.40 numerical aperture oil-immersion objective and Kodak T-Max 100 (for Calcofluor staining) or T-Max 400 (for Cdc11p and Aip3p immunofluorescence) film.

For immunolocalization of Aip3p, cells growing exponentially in liquid culture at 30°C were pelleted and resuspended in 1 ml of phosphate-buffered saline (PBS) containing 0.035% glutaraldehyde. After 3 min, the cells were pelleted and resuspended in 1 ml of PBS containing 3.7% formaldehyde. After 10 min, the cells were pelleted and resuspended in 1 ml of acetone and then incubated for 2 min at −20°C. Cells were then washed twice in solution A [40 mM potassium phosphate, pH 6.5, 0.5 mM $MgCl_2$, 1.2 M sorbitol (Pringle *et al.*, 1989)] followed by treatment with yeast lytic enzyme (ICN; 0.5 mg/ml) and 2-mercaptoethanol (1%) in solution A for 1 h at 37°C to remove cell walls. The cells were then washed once in PBS containing 1% bovine serum albumin and applied to polylysine-coated slides. Purified anti-Aip3p antibody was applied undiluted to each well and incubated for 1 h at room temperature or overnight at 4°C. The cells were then washed ten times with PBS containing 1% bovine serum albumin, incubated in BODIPY-FL-conjugated goat anti-rabbit IgG (heavy and light chains) antibody (Molecular Probes) diluted 1:200, and incubated for 1 h at room temperature. The cells were then washed as described above and mounted in 90% glycerol containing *p*-phenylenediamine at 1 mg/ml (Pringle *et al.*, 1989).

Cells expressing the GFP-Aip3p fusion protein were observed either by conventional fluorescence microscopy using the fluorescein isothiocyanate filter set or by time-lapse video microscopy. For the latter experiments, strain YEF473 containing plasmid pRB2190 was grown overnight to mid-exponential phase in liquid SC-Ura medium at room temperature. Cells were sonicated briefly to disrupt clumps (Pringle and Mor, 1975) and applied to microscope slides coated with SC-Ura medium containing 25% gelatin. Coverslips were applied and sealed with Valap (1:1:1 Vaseline:lanolin:paraffin), and cells were observed at room temperature on a Nikon Microphot FXA microscope equipped with a Hamamatsu cooled charge-coupled device camera and an Apo 60×/1.4 numerical aperature oil-immersion objective in combination with a 1.25× Optivar. Images were collected every 2 min using a 600-ms exposure of 490-nm light. Images were collected and analyzed using the Universal Metamorph Imaging System.

Electron Microscopy

A 100-ml culture of exponentially growing cells (5×10^6 cells/ml) in YPD:2% glucose medium was quickly concentrated by vacuum filtration to a total volume of about 5 ml. To this concentrated cell suspension, 25 ml of freshly prepared fixative [40 mM potassium phosphate, pH 6.7, 0.8 M sorbitol, 4% methanol-free formaldehyde (Thorne *et al.*, 1975) freshly prepared from paraformaldehyde (Polysciences, Warrington, PA), 0.4% glutaraldehyde (EM grade; Polysciences), 1 mM $MgCl_2$, 1 mM ethylene glycol-bis(β-aminoethyl ether)-*N,N,N',N'*-tetraacetic acid, pH 8) at room temperature was added and mixed rapidly with the cells. The cell suspension was then incubated at room temperature for 1 h. The fixed cells were then washed out of the fixative and processed for immunoelectron microscopy exactly as described by Mulholland *et al.* (1994).

RESULTS

Identification of AIP3/BUD6

We described previously the isolation of proteins capable of interacting with yeast actin in the two-hybrid system (Amberg *et al.*, 1995a). Yeast actin was fused to the DBD of Gal4p and used to screen a library of yeast cDNAs fused to DNA encoding the Gal4p AD. This screen identified well-known or suspected actin-binding proteins including actin itself, profilin, Srv2p, and Rvs167p. These results confirmed that the actin portion of the actin-Gal4p-DBD fusion protein was correctly folded and able to bind authentic actin ligands. In addition, we identified three previously undescribed proteins we called Aip1p, Aip2p, and Aip3p (actin-interacting proteins 1, 2, and 3).

AIP3 was the most frequently identified gene in the screen: four clones that proved to contain different portions of the ORF were identified (Figure 1). The *AIP3* cDNA insert was excised in a 1-kb *Bgl*II fragment (sites in the vector sequences) from plasmid pRB2186, radiolabeled, and used to map *AIP3* physically. This fragment hybridized to λ′ clones 3681 and 3929 (ATCC 70204 and 70235), localizing *AIP3* to the vicinity of *CDC3* on chromosome XII. Comparison of cDNA sequence from the *AIP3* ORF to the chromosome XII sequence (Johnston, personal communication) identified *AIP3* as ORF YLR319C.

Independently, we cloned the *BUD6* gene, as identified by a mutation (*bud6–1*) that disrupts the bipolar budding of **a**/α cells but does not affect the axial budding of **a** or α cells (Figure 2, A and C) (Zahner *et al.*, 1996). An **a**/α *bud6–1/bud6–1* strain (YJZ233) was transformed with a yeast genomic DNA library in the YCp50-LEU2 shuttle vector (see MATERIALS AND METHODS). Individual transformants were stained with Calcofluor and examined microscopically, as described previously (Zahner *et al.*, 1996). One transformant was identified that showed normal bipolar budding. Plasmid was recovered from this transformant and fragments were subcloned into the YCplac111 shuttle vector. This revealed that a 3.3-kb *Hin*dIII fragment (plasmid YCp111/H3.3) was able to restore normal budding pattern as well as normal cell morphology (see below) to the *bud6–1/bud6–1* strain (Figure 2, C and D). Physical mapping showed that the 3.3-kb *Hin*dIII fragment hybridized to λ′ clones 3681 and 3929 from the *CDC3* region of chromosome XII, near where the *bud6–1* mutation had been mapped (Zahner *et al.*, 1996). Sequencing of the 3.3-kb *Hin*dIII fragment revealed one complete ORF identical (except in a few positions; see Figure 1 legend) to ORF YLR319C of the chromosome XII sequence. Disruption of this ORF (de-

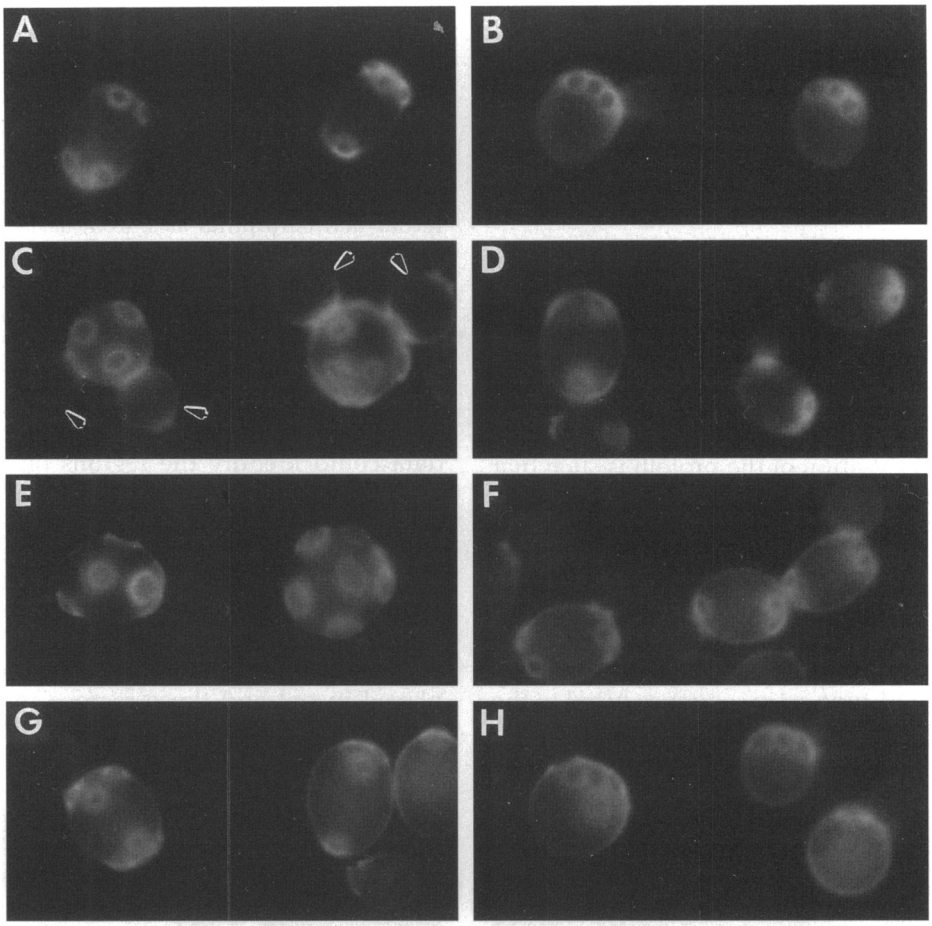

Figure 2. Budding pattern phenotypes of wild-type and mutant strains and rescue of mutant phenotypes by *AIP3/BUD6* plasmids. Cells growing exponentially in YM-P liquid medium were fixed and stained with Calcofluor to visualize bud scars. (A) Wild-type diploid strain YEF473 with normal bipolar budding. (B) Wild-type haploid strain YEF473B with normal axial budding. (C) Diploid *bud6–1/bud6–1* strain YJZ233 with random distribution of bud scars (and other morphological abnormalities, see text; arrowheads indicate the attached buds or daughter cells). (D) YJZ233 harboring plasmid YCp111/H3.3, showing restoration of bipolar budding (and normal morphology). (E) Diploid *aip3*-Δ3/*aip3*-Δ3 strain YJZ358 with phenotype similar to that of YJZ233. (F and G) YJZ358 harboring plasmid YCp111/H3.3 (F) or pRB2190 (encoding GFP-Aip3p) (G), showing rescue of the mutant phenotypes. (H) Haploid *aip3*-Δ3 strain YJZ356 with normal axial budding.

scribed below) produced a mutation (*aip3*-Δ3::*TRP1*) whose phenotype was similar to that of *bud6–1* (Figure 2, C and E) and that failed to complement *bud6–1* (i.e., the diploid formed by mating a disruption strain to a *bud6–1* strain resembled the *bud6–1/bud6–1* strain in budding pattern and morphology). The noncomplementation and coincidence of map position demonstrate that ORF YLR319C is the bona fide *BUD6* gene; these data thus also establish the identity of *BUD6* and *AIP3*. For most of what follows, the *AIP3* name will be used.

Analysis of the AIP3 Sequence

The predicted Aip3p sequence is represented diagrammatically in Figure 1. The ORF extends well upstream of the largest two-hybrid clones and is predicted to encode a 788-amino acid, 89-kDa protein, consistent with the apparent size of Aip3p as observed by Western blotting (see below). No close homologues of Aip3p were detected in GenBank. Aip3p does have some weak similarities to many proteins including desmoplakin ($p = 0.00053$), a major component of desmosomal plaques (Schmidt *et al.*, 1994); restin ($p = 0.00093$), an intermediate filament-associated protein (Bilbe *et al.*, 1992); Mlp1 ($p = 0.0015$), a coiled coil protein of unknown function (Kölling *et al.*, 1993); and a long list of myosin heavy chains. Interestingly, many of these proteins are bona fide components of the cytoskeleton but have little else in common. More striking is the observation that virtually all of the homologues are coiled-coil proteins. The region of highest homology between Aip3p and these coiled-coil proteins is in

the C-terminal half of Aip3p, the same region that interacts with actin in the two-hybrid assay, and the empirical program of Lupas *et al.* (1991) predicts that amino acids 565–628 of Aip3p are a coiled-coil domain (see Figure 1).

Differential Interactions between Mutant Actins and Aip3p

One way to describe how two proteins contact each other is to determine the distribution of mutations that affect their ability to interact. Such an analysis is particularly informative when the three-dimensional structure of at least one of the proteins is available along with a large set of mutations affecting most of the surface of that protein. These criteria are met for yeast actin: the conservation of the protein is such that the crystallography studies on mammalian actin suffice to make credible models of yeast actin, and a suitable set of mutations in yeast actin has been constructed (Wertman *et al.*, 1992).

We used the two-hybrid system to assess the ability of mutations in actin to affect binding to Aip3p, as described previously for other actin ligands (Amberg *et al.*, 1995a). The wild-type actin sequence fused to the Gal4p-DBD was replaced with various mutant actin sequences, and each actin variant was then assessed for its ability to interact with fusions of Aip3p to the Gal4p-AD. The results, read as degree of activation of a Gal4p-responsive promoter driving His3p expression, as assessed by the ability to grow in the presence of aminotriazole, define "differential interactions" (Amberg *et al.*, 1995a). By this assay, the recessive lethal actin mutants *act1–103*, *act1–131*, and *act1–134* and the conditional actin mutants *act1–119* and *act1–124* (tested at the permissive temperature of 30°C) failed completely to interact with constructs containing Aip3p sequences, and actin mutants *act1–120*, *act1–133*, and *act1–123* displayed compromised interactions.

We then asked whether the differential-interaction data could identify the regions on actin involved in binding Aip3p. Figure 3 shows the calculated solvent-exposed surface of front (Figure 3A) and back (Figure 3B) views of actin; the actin structure is adapted from the coordinates for mammalian actin (Kabsch *et al.*, 1990) as described previously (Amberg *et al.*, 1995a). Those regions of the actin surface that, when altered by mutation, eliminate the binding of Aip3p are displayed in red and those regions in which mutations weaken the interaction are displayed in blue. (Note

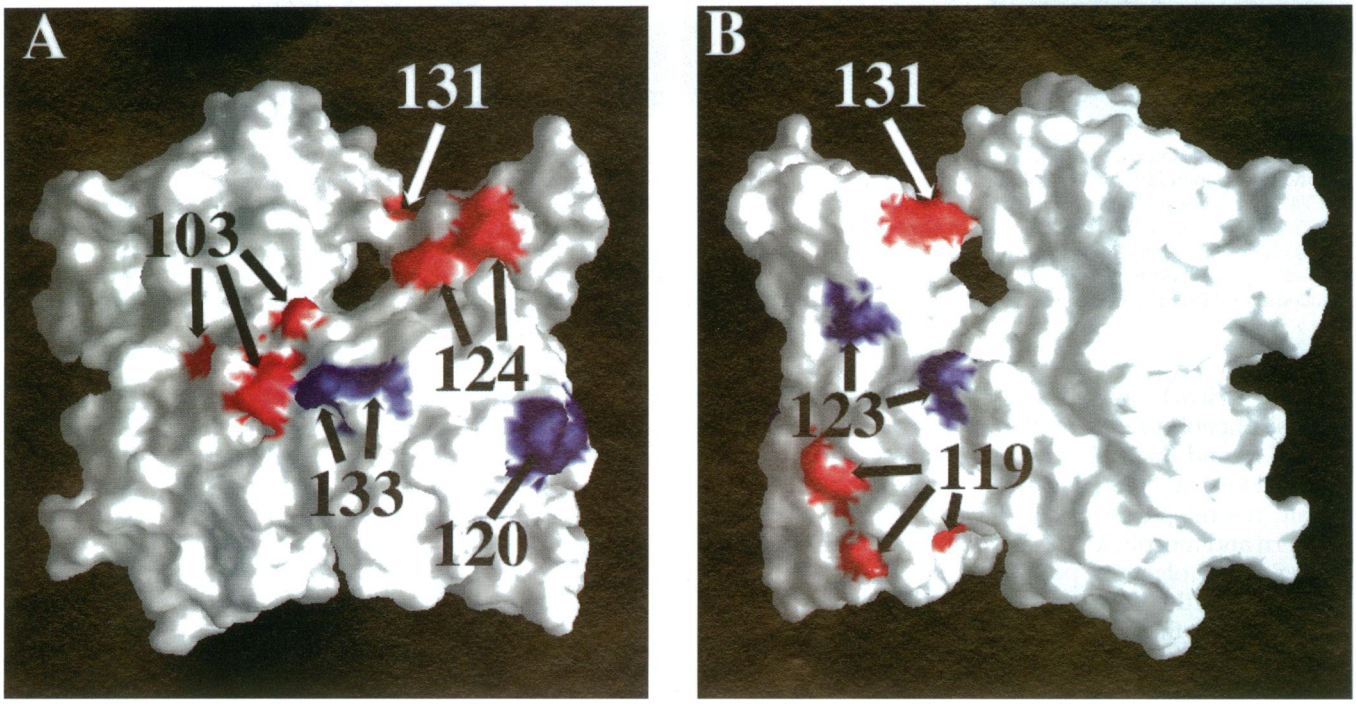

Figure 3. Binding footprint for Aip3p on actin. The solvent-exposed surface of rabbit muscle actin was calculated by using GRASP software on a Silicon Graphics Iris computer. The front (largely solvent-exposed in F-actin) surface is displayed in A and the back (largely buried in F-actin) surface is displayed in B. The amino acid side chains of residues altered by mutations that eliminate the actin-Aip3p interaction (*act1–103*, *act1–119*, *act1–124*, and *act1–131*) are displayed in red, whereas those mutations that appear only to weaken the interaction (*act1–120*, *act1–123*, and *act1–133*) are shown in blue. Mutation *act1–134* alters entirely buried residues in subdomain 1 and is, therefore, not visible in this rendering.

that mutation *act1–134* alters entirely buried residues within subdomain 1 and, therefore, is not visible in this surface rendering.) Because we expect that some mutations may cause more than localized disturbances in the actin structure, we feel that these data are best interpreted as indicating regions of the molecule whose integrity is important for the interaction. It is not possible by these methods to identify definitively the binding residues.

This footprint for Aip3p is less easy to interpret than the footprints we obtained for many other ligands. The disruptive mutations are located on both the front and back surfaces of actin but tend to cluster on subdomains 1 and 2. Mutation *act1–131* disrupts a salt bridge (in the model of Kabsch *et al.*, 1990) that holds the two halves of the molecule together, suggesting that binding by Aip3p requires that the two domains be correctly oriented with respect to each other. Mutation *act1–119* disrupts nearly all interactions with actin in the two-hybrid system, indicating that it may disturb, in a more general way, the structure of at least subdomain 1. In contrast, mutations *act1–103* and *act1–124* disrupt the binding of only two and three, respectively, of the other proteins we tested, and therefore, we believe that they disrupt the Aip3p-actin interaction by causing localized disturbances on the surface of actin. Collectively, these observations lead us to hypothesize that Aip3p binds across the front surface of the two halves of actin, probably contacting subdomains 1, 2, and 3. This view is consistent with the possibilities that Aip3p interacts with polymerized actin, monomer actin subunits, or both. It is significant that binding to filaments is not ruled out, as it was for proteins such as profilin, Srv2p, Oye2p, and Aip2p (Amberg *et al.*, 1995a; our unpublished results).

Interaction of Aip3p with Itself

We also used the two-hybrid system to determine whether Aip3p could interact with itself. The *AIP3* insert from pRB2187 (see Figure 1) was fused to the Gal4p-DBD sequences, and the product of this fusion gene was tested for its ability to interact with the products of the four cDNA clones bearing fusions of Aip3p to the Gal4p-AD (see Figure 1). Figure 4 shows the results of this analysis. The large Aip3p fusion to the Gal4p-DBD interacted with three of the four fusions of Aip3p to the Gal4p-AD. The clone that failed to interact, Aip3p(540–788), carries 18 more amino acids of Aip3p than does a clone, Aip3p(558–788), that did interact. Perhaps the context of the fusion in Aip3p(540–788) interferes with the Aip3p-Aip3p interaction.

This analysis is consistent with the Aip3p C terminus having the capacity to interact with itself in addition to carrying an actin-interacting domain. It remains possible that the C terminus of the shorter fusion is interacting with the N-terminal portion of the longer fusion; however, the sequence characteristics of the C-terminal region suggest that the interaction may occur via a coiled-coil interaction in which the C-terminal portions of two (or possibly more) Aip3p proteins self-associate.

Characterization of aip3Δ Strains

To determine the consequences of a loss of Aip3p function, we constructed three different *AIP3* deletion alleles, two (*aip3-Δ1* and *aip3-Δ2*) in the DBY6525 background and one (*aip3-Δ3*) in the YEF473 background (Figure 1; see MATERIALS AND METHODS). Many features of the *aip3-Δ* phenotype were similar or identical among the different strains, whereas other features appeared to be affected by the genetic background. In what follows, we describe the common features of the phenotype and also indicate some of the variability that has been observed.

Growth Rates and Viability. All of the deletion strains were viable and could grow in medium of either nor-

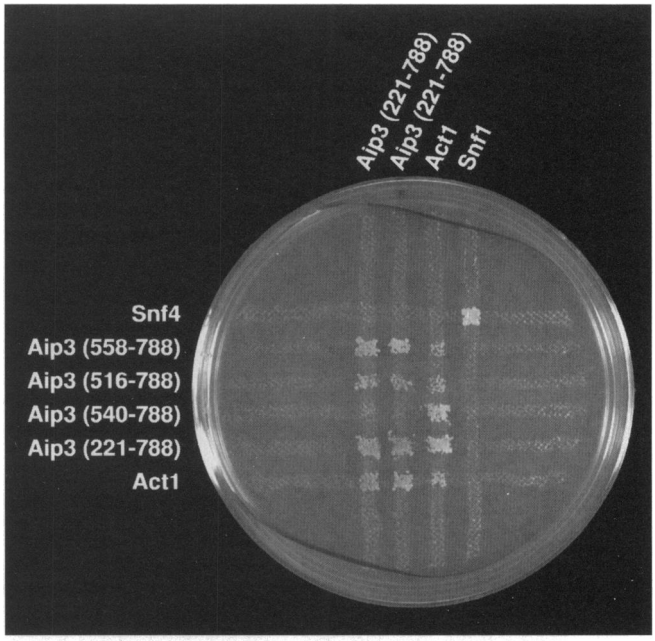

Figure 4. Interaction of Aip3p with itself in the two-hybrid system. Yeast strain DBY5651 carrying fusions to the Gal4p-DBD (vertical streaks) of Aip3p amino acids 221–788 (pRB2188 and pRB2189, two independent isolates), Act1p (actin; pRB1516), and Snf1p (pRB1505) were mated to yeast strain DBY5650 carrying fusions to the Gal4p-AD (horizontal streaks) of Snf4p (pRB1504), Aip3p amino acids 558–788 (pRB2184), Aip3p amino acids 516–788 (pRB2185), Aip3p amino acids 540–788 (pRB2186), Aip3p amino acids 221–788 (pRB2187), and Act1p (pRB2146). Diploids bearing both plasmid types were selected at the intersections on medium lacking tryptophan and leucine and then replica plated to medium containing 50 mM 3-aminotriazole to test for interaction of the fusion partners. The Act1p, Snf1p, and Snf4p constructs provide positive and negative controls.

mal or high (0.9 M NaCl) osmolarity, but their growth was compromised to various extents. The *aip3-Δ1* and *aip3-Δ2* strains grew slightly more slowly (and with more heterogeneity in colony size) than the related wild-type strains at 18 and 25°C, and growth of the mutants was more severely compromised at 30 and 37°C (Figure 5). In addition, *aip3-Δ2* strains grew more poorly than did the *aip3-Δ1* strains, and the homozygous mutant diploids were affected more severely than were the mutant haploids (Figure 5). The reduced growth rates were correlated with relatively high levels of inviable cells in the populations: in liquid cultures of strains DBY6937 (*aip3-Δ1*), DBY7055 (*aip3-Δ2*), DBY6939 (*aip3-Δ1/aip3-Δ1*), and DBY7057 (*aip3-Δ2/aip3-Δ2*) grown at 30°C, there were 16, 22, 28, and 48% inviable cells, respectively, in comparison to essentially none in the congenic wild-type strains DBY6924 and DBY6525. The difference in growth rates between the *aip3-Δ2* and *aip3-Δ1* strains suggests that the truncated protein encoded by *aip3-Δ1* (the N-terminal 292 amino acids, or ~37% of the normal polypeptide) might provide partial Aip3p function. On the other hand, the *aip3-Δ3* strains YJZ356 and YJZ358, which should also completely lack Aip3p function, grew only slightly more slowly than the congenic wild-type strains YEF473B and YEF473 at temperatures from 18 to 37°C and displayed homogeneous colony sizes and <10% inviable cells in medium of normal osmolarity. In contrast, inclusion of 0.9 M NaCl in the medium slowed the growth of YJZ358 substantially (relative to that of YEF473) but had a more modest effect on the growth of DBY6939 and DBY7057. Thus, a loss of Aip3p function retards growth and reduces cell viability, but the extent of these effects ranges from slight to severe depending on the genetic background, ploidy, and growth conditions.

Morphology and Actin Organization. Like the original *bud6–1* mutant (Figure 2C), all of the *aip3Δ* strains display rounder cells, more heterogeneity in cell size (an effect that is more pronounced with the *aip3-Δ1* and *aip3-Δ2* strains than with the *aip3-Δ3* strains), thicker mother-bud necks, and (consequently) larger bud scars than the related wild-type strains (Figures 2, A, B, E, and H, and 6B; the effects of *aip3* mutations on budding pattern are discussed below). The *aip3* mutants also frequently form clusters or chains of cell bodies (Figures 2C and 6B), suggesting a delay in cytokinesis or cell separation. The observation that many clusters or chains remain when fixed cells are treated with cell-wall-digesting enzymes (Pringle and Mor, 1975) indicates that there is in fact a delay or failure of cytokinesis, at least in some cells, a conclusion that is supported by the electron microscopy observations described below. All of these morphological abnormalities, as well as the effects on actin organization described below, are corrected by introducing wild-type *AIP3* on a low copy number plasmid (see Figure 2, D and F).

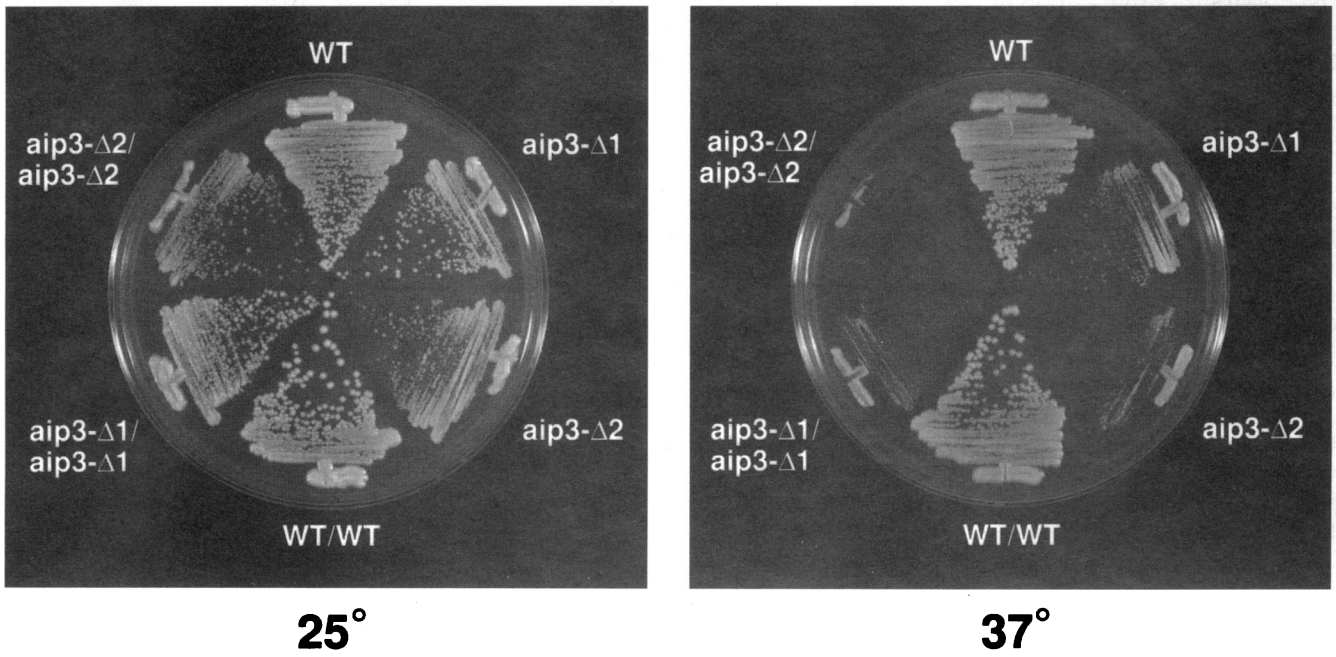

Figure 5. Effects of *AIP3* deletion on growth rate. Haploid and diploid strains either wild-type or mutant at *AIP3* were streaked on YPD solid medium and incubated at 25°C or 37°C as indicated. The strains shown are DBY6924 (WT), DBY6925 (WT/WT), DBY6937 (*aip3-Δ1*), DBY6939 (*aip3-Δ1/aip3-Δ1*), DBY7055 (*aip3-Δ2*), and DBY7057 (*aip3-Δ2/aip3-Δ2*). The *aip3-Δ3* mutation (in the YEF473 background) had a much more modest effect on growth rate (see text).

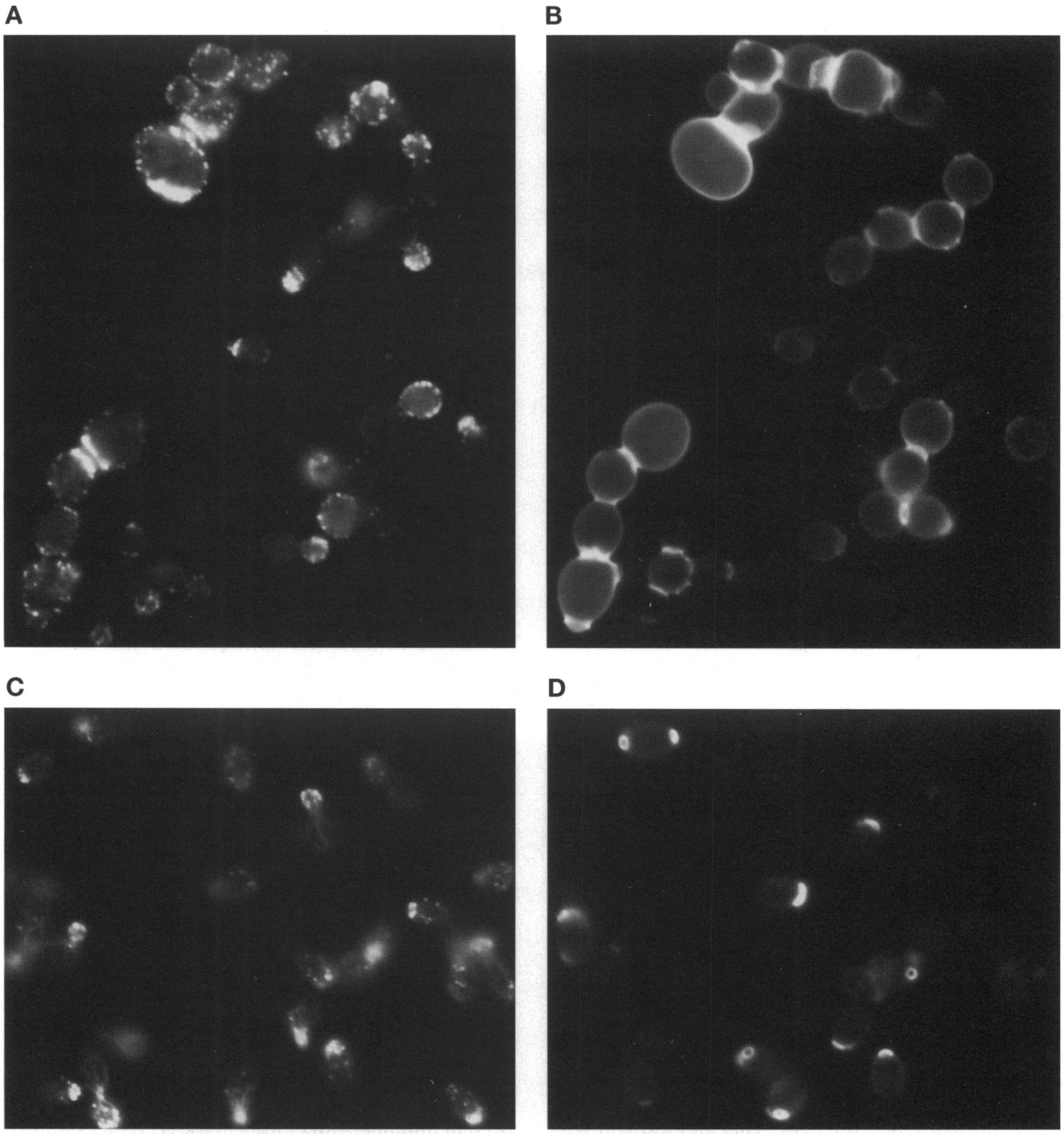

Figure 6. Depolarization of the actin cytoskeleton in *aip3*Δ strains. Wild-type strain DBY6525 (C and D) and *aip3*-Δ*1*/*aip3*-Δ*1* strain DBY6939 (A and B) were grown into early exponential phase at 30°C, fixed with formaldehyde, and stained with rhodamine-phalloidin to visualize the actin cytoskeleton (A and C) and with Calcofluor to visualize patterns of chitin deposition (B and D).

The presence of cells that are larger and rounder than normal suggests a partial defect in the polarization of cell growth. Consistent with this possibility, staining of the *aip3*Δ cells with rhodamine-phalloidin revealed a partial loss of polarization of the actin cytoskeleton. In contrast to wild-type cells (Figure 6C),

*aip3*Δ cells displayed few, if any, detectable actin cables (Figure 6A). In addition, although the cortical actin patches were concentrated more or less normally in the buds of *aip3*Δ cells with small buds, there were often some patches in the mother cells as well; this effect was typically more pronounced in cells with larger buds, and some cells appeared to be quite depolarized for actin-patch localization (Figure 6A). A further indication of a partial loss of growth polarization is that the *aip3* mutant cells (at least in the *aip3-Δ1* and *aip3-Δ2* strains) often appeared to have some delocalized chitin deposition, as indicated by Calcofluor staining that was not confined to the bud scars (Figure 6B), although the vagaries of Calcofluor staining (Pringle *et al.*, 1989) make it difficult to establish this effect convincingly. Interestingly, although actin became concentrated at the necks of *aip3*Δ cells late in the cell cycle, as in wild-type strains, these actin concentrations often appeared exaggerated (Figure 6A), perhaps reflecting a delay in the cell cycle at this stage (see below).

The relatively modest changes in overall growth rate and viability described above might result either from minor defects in a growth process that normally occupies a large fraction of the cell cycle or from a more major defect in a process that normally occupies a small fraction of the cell cycle. To ask whether mutation of *AIP3* affected cell cycle kinetics, we examined *aip3-Δ1* and *aip3-Δ2* cells using antitubulin immunofluorescence in conjunction with DAPI staining of DNA and visualization of cell bodies by DIC microscopy. Approximately 300 cells of each strain were scored. In the wild-type control strains, 15–20% of the cells contained mitotic spindles of various lengths, whereas spindles were observed in 30–40% of the *aip3* mutant cells. Although some variation was observed between *aip3-Δ1* and *aip3-Δ2* cells, between haploids and diploids, and between cells grown at 25 or 37°C, consistently twice as many cells were in mitosis in the *aip3* mutants as in the wild-type controls. Thus, the growth-rate differences (20–50%) in the *aip3*Δ strains may result at least in part from a substantial defect (twofold) in a late mitotic process. In the cells with long spindles, the DAPI staining indicates that the DNA is well separated, suggesting that the cells may have difficulty in disassembling their spindles. In some of the cells, the spindles were located entirely in the mother cell, suggesting that the spindle cannot move efficiently into the neck. This may explain why many cells in the *aip3-Δ1* and *aip3-Δ2* populations (18/301, or 6%, in a count on strain DBY6939) have two or more nuclei. The effect on nuclear segregation appears to be dependent on genetic background, as strain YJZ358 (*aip3-Δ3/aip3-Δ3*) contained very few cells with two or more nuclei.

Budding Pattern. Like the original *bud6–1* mutation (Figure 2C; Zahner *et al.*, 1996), the *aip3*Δ mutations disrupt the bipolar budding pattern of **a**/α cells (Figure 2E) but do not detectably affect the axial budding pattern of **a** or α cells (Figure 2H). As with the other morphological abnormalities described above, the effect on budding pattern was reversed by introducing wild-type *AIP3* on a low copy number plasmid (Figure 2F). To examine the effects on budding pattern in more detail, we scored the positions of first, second, and third buds in strain YJZ358 (*aip3-Δ3/aip3-Δ3*) and the congenic wild-type strain YEF473. As in the wild-type strain (Figure 7A; see also Chant and Pringle, 1995; Zahner *et al.*, 1996), daughter cells of the *aip3-Δ3/aip3-Δ3* strain placed their first buds predominantly at the distal pole (Figure 7B). However, these first bud sites were less frequently at the very tip of the distal pole in the mutant strain than in the wild-type strain (Figure 7C; see also Chant and Pringle, 1995; Zahner *et al.*, 1996). Moreover, whereas the wild-type cells continued to bud predominantly from the two poles in later cell cycles, with a gradual loss of bias for the distal pole (Figure 7A), the mutant cells appeared to select bud sites at random in their second and subsequent cell cycles (Figure 7B). When a mutant cell did produce both of its first two buds at the distal pole, the bud sites were generally not directly adjacent to each other, in contrast to the situation in wild-type cells (Chant and Pringle, 1995; Zahner *et al.*, 1996).

Ultrastructure. To investigate the morphological abnormalities of *aip3*Δ strains at an ultrastructural level, an exponentially growing culture of strain DBY6939 (*aip3-Δ1/aip3-Δ1*) was prepared for immunoelectron microscopy with anti-actin antibodies (see MATERIALS AND METHODS). A sample of the images is presented in Figure 8. Three types of defects were observed.

First, as suggested by the light microscopic observations, the septa of *aip3-Δ1* cells are often abnormal, and sometimes grossly so (Figure 8A). Many septa are thick and exaggerated and have pockets of cytoplasm containing large amounts of actin. In some cases, channels of cytoplasm were observed going through the septa such that the cells were not completely separated.

Second, several observations suggest that there are secretory defects in the *aip3-Δ1* cells. The aberrant cells display abundant vesicles that are heterogeneous in size and appearance, as well as clumps of vesicles and abnormal-appearing membranes, similar to structures seen in mutants with defects in the secretory pathway or in the actin cytoskeleton (Mulholland, unpublished observations). An example of an actin-containing membranous aggregate such as those sometimes seen in actin mutants is shown in Figure 8A (left of the septum); such structures are also observed in *sec7* mutants (Mulholland, unpublished observations). Some cells show a ballooning of the endoplasmic reticulum that is extreme even for secretory mutants

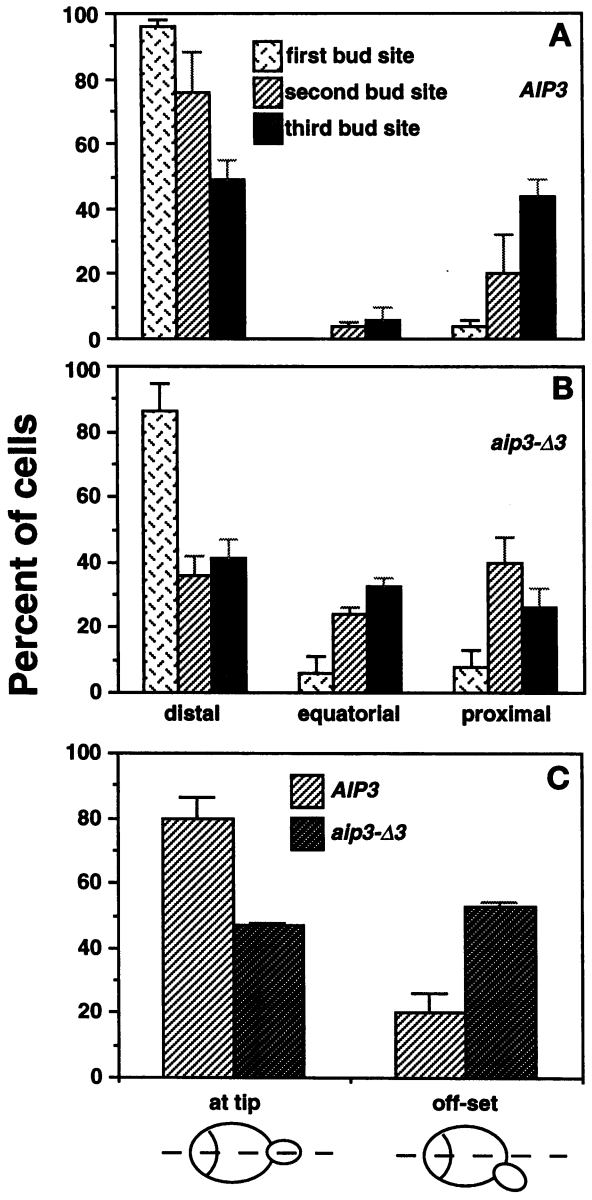

Figure 7. Effect of *AIP3* deletion on the bipolar budding pattern; the *aip3*-Δ3/*aip3*-Δ3 strain YJZ358 (B and C) is compared with the congenic wild-type strain YEF473 (A and C). Three independent cultures of each strain were grown in YM-P liquid medium at 30°C to mid-exponential phase, fixed with formaldehyde, and stained with Calcofluor to visualize both birth and bud scars. Each histogram represents the average values and the error bars indicate the ranges in values from the three cultures. (A and B) In each experiment, 100 cells with no bud scars, 100 cells with one bud scar, and 100 cells with two bud scars were scored for whether newly formed buds (i.e., first, second, and third buds, respectively) were in the distal, equatorial, or proximal third of the cell surface; the proximal pole was identified by the birth scar. (C) In each experiment, 100 cells with no bud scars and a single bud in the distal third of the cell surface were scored for whether the bud was at the very tip of the distal pole (defined as the point directly opposite the center of the birth scar; see diagram) or detectably offset from the tip.

(Figure 8A, lower left). In addition, there is often a deficiency in the accumulation of late secretory vesicles in small buds (Figure 8, B and C). Both of the small budded cells shown have cortical actin patches localized to the bud neck, but the buds contain very few 70–100-nm vesicles. Previous work has demonstrated that such small buds normally contain a large concentration of membranous material and late-stage secretory vesicles (Preuss *et al.*, 1992; Mulholland *et al.*, 1994).

Third, we have frequently observed bars of actin in the nuclei of these cells. Actin bars were first observed in *act1–2* mutant cells and have subsequently been observed in other actin mutants and in mutants defective in actin-binding proteins (Novick and Botstein, 1985; our unpublished observations). Such bars are typically located in the cytoplasm, and it was surprising to find them in the nuclei of *aip3*-Δ*1* cells. The significance of this observation is unclear.

Localization of Aip3p

We used two methods to investigate the intracellular localization of Aip3p and its changes through the cell cycle. For localization by immunofluorescence, we raised antibodies against a MBP-Aip3p fusion protein. Antibodies recognizing Aip3p were affinity purified and further purified by adsorption of unwanted antibodies to cells of an *aip3*-Δ*3* strain (see MATERIALS AND METHODS). When tested on Western blots of yeast proteins, the purified antibodies recognized several polypeptides in extracts of wild-type haploid or diploid cells (Figure 9, lanes 2 and 5), including a polypeptide with an apparent molecular mass of ~97 kDa, consistent with the predicted size of Aip3p (see above). This polypeptide indeed appears to be Aip3p, as it is absent in extracts of *aip3*-Δ3 cells (Figure 9, lanes 1 and 4) and more abundant (along with several presumed breakdown products) in extracts of cells harboring a high-copy *AIP3* plasmid (Figure 9, lanes 3 and 6).

When the purified antibodies were used for immunofluorescence on wild-type cells (Figure 10A) or cells harboring a high copy number *AIP3* plasmid (Figure 10B), similar patterns of localized staining were observed. This staining was typically brighter and visible in a higher proportion of the cells in the Aip3p-overexpressing cells, and no such localized staining was observed with *aip3*-Δ*3* cells (Figure 10C), indicating that the patterns observed in wild-type and Aip3p-overexpressing cells indeed represent the localization of Aip3p and not that of cross-reacting proteins. Many unbudded cells and cells with very small buds displayed a single bright patch of Aip3p staining (Figure 10, A and B, white arrowheads). In the cells with buds, these patches of staining were at the bud sites, and they are inferred to be at the incipient bud sites on the

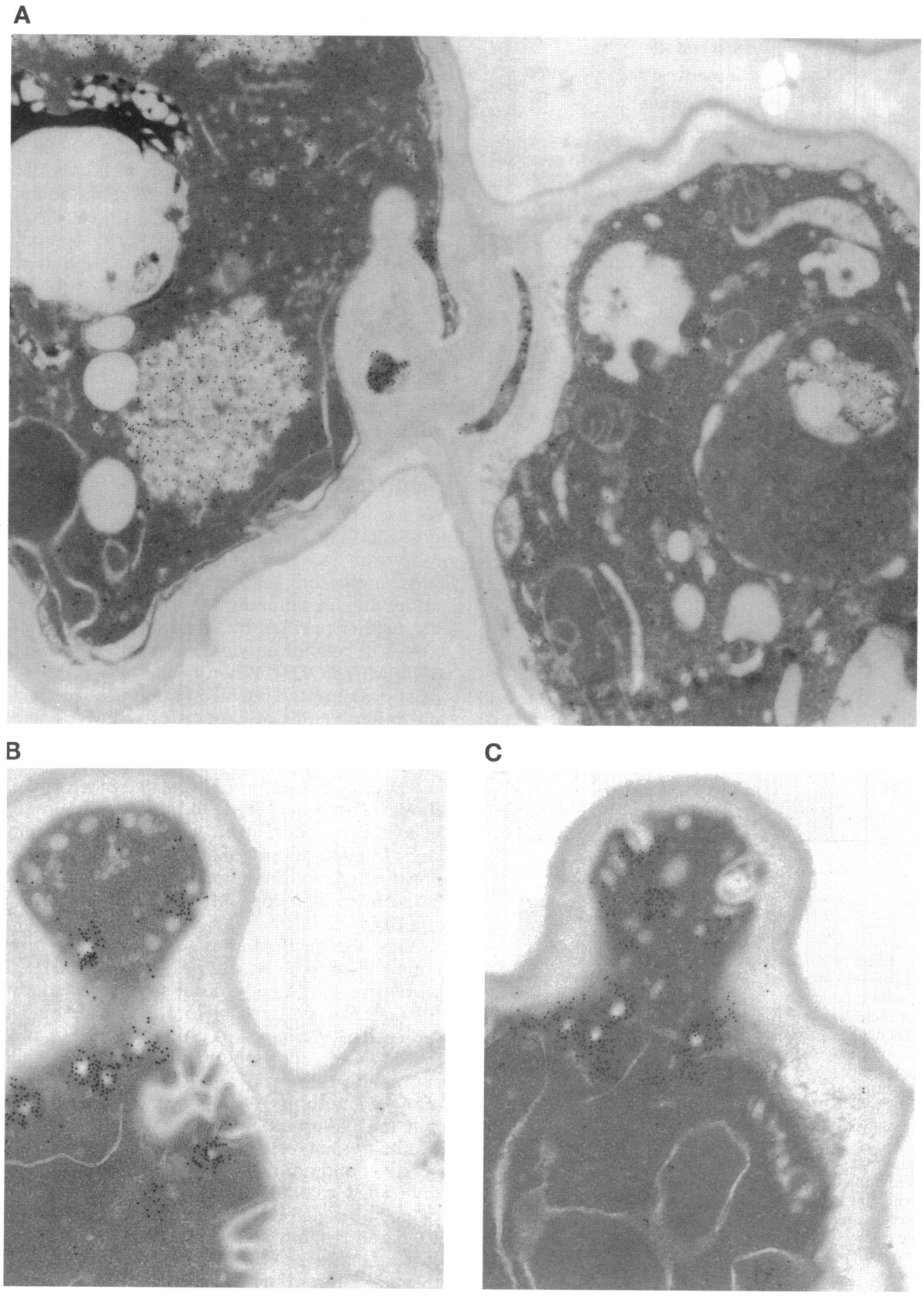

Figure 8.

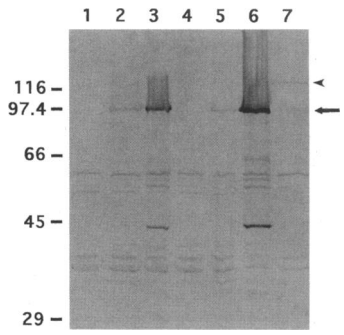

Figure 9. Western blot of yeast proteins probed with purified anti-Aip3p antibodies (see MATERIALS AND METHODS). The molecular masses of marker proteins are indicated on the left (in kDa). The arrow and arrowhead indicate the mobilities of Aip3p and the GFP-Aip3p fusion protein, respectively. Lane 1, haploid *aip3*-Δ3 strain YJZ356; lane 2, haploid wild-type strain YEF473B; lane 3, YEF473B harboring *AIP3* plasmid YEp352/H3.3; lane 4, diploid *aip3*-Δ3/*aip3*-Δ3 strain YJZ358; lane 5, diploid wild-type strain YEF473; lane 6, YEF473 harboring *AIP3* plasmid YEp352/H3.3; lane 7, YEF473 harboring GFP-*AIP3* plasmid pRB2190. Cells were grown in YM-P medium (strains without plasmids) or in SC-Ura medium (strains with plasmids).

unbudded cells from their singularity (one per cell), location near a pole of the cell, and similarity to the patches seen on cells with very small buds. In cells with medium-sized buds, one or a few patches of staining were typically observed near the tip of the bud (Figure 10, A and B, white arrows), sometimes accompanied (generally in cells with relatively large buds) by a faint ring (or double ring) of staining at the mother-bud neck (Figure 10, A and B, single black arrowheads). In cells with large buds, the apparent double ring of staining at the mother-bud neck was typically much brighter (Figure 10, A and B, double black arrowheads) and unaccompanied by patches of staining near the tip of the bud. Some unbudded cells also displayed a band or ring of staining that appeared to represent residual Aip3p localization to the preceding division site (Figure 10B, black arrows). Indistinguishable staining patterns were observed with haploid cells (strain YEF473B; our unpublished data).

To confirm and extend the results of immunofluorescence, we created a fusion of the *Aequorea victoria* green fluorescent protein (GFP) (Chalfie *et al.*, 1994) to the N terminus of Aip3p. The fusion gene was under the control of the *ACT1* promoter and terminator in the low copy number plasmid pRB2190. When pRB2190 was introduced into wild-type diploid strain YEF473 and extracts were examined using Western blotting, a novel polypeptide was observed with an apparent molecular mass of ~122 kDa, as expected for the GFP-Aip3p fusion protein (Figure 9, lane 7). The amount of this polypeptide appeared to be similar to that of Aip3p itself, indicating that the fusion protein was not grossly overproduced. When pRB2190 was introduced into the *aip3*-Δ2/*aip3*-Δ2 strain DBY7057 or the *aip3*-Δ3/*aip3*-Δ3 strain YJZ358, it largely restored cell morphology, cytoskeletal organization, and budding pattern to normal (Figure 2G and our unpublished data). However, the fusion protein was unable to restore a wild-type growth rate to strains carrying the *aip3*-Δ1 or *aip3*-Δ2 allele. As plasmids carrying full-length genomic copies of *AIP3* fully rescued all phenotypes (Figure 2F), it appears that the GFP-Aip3p fusion protein supplies much, but not all, of the function of normal Aip3p.

When pRB2190 was introduced into wild-type diploid strain DBY2565 and the cells were examined by conventional fluorescence microscopy, the patterns of protein localization observed were very similar to those seen by immunofluorescence (Figure 11, A–D). Unlike the actin cortical patches, which are highly dynamic (Doyle and Botstein, 1996; Waddle *et al.*, 1996), the cortical spots of GFP-Aip3p in medium-sized buds did not appear to move much when observed in real time. This observation suggests that the GFP-Aip3p spots do not in fact correspond to the actin cortical patches, a suggestion supported by observations on cells expressing GFP-Aip3p and stained with rhodamine-phalloidin (our unpublished results).

Taking the results of the immunofluorescence and GFP-Aip3p localization together, it appears that Aip3p becomes concentrated at the incipient bud site prior to bud emergence, remains concentrated in patches in the bud (usually near their tips) for at least part of the period of bud growth, and also becomes concentrated some time after bud emergence in a band at the mother-bud neck that can remain to mark the division site after cell division. There may be two discrete stages in the development of the band of Aip3p at the neck, as a faint and apparently single ring of signal present in cells with relatively small buds (Figure 11D) is succeeded by a much stronger and apparently double ring of signal in cells with larger buds (Figures 10, A and B, and 11A). Interestingly, in at least some mother cells, the concentration of Aip3p to the next bud site appears to occur very early, perhaps even before completion of the previous division (Figures 10A, cell marked by *, and 11B).

To explore further the localization of Aip3p through the cell cycle, we examined living cells expressing the GFP-Aip3p fusion protein by low-light–level video-enhanced time-lapse microscopy (see MATERIALS AND METHODS). There are three significant caveats to the interpretation of these experiments. First, it is clear that the cells were not growing completely normally under the conditions of observation. For example, although mother cells normally bud again before their daughters bud (Pringle and Hartwell, 1981), the two mother cells in the lower part of the cluster shown in Figure 12 never budded again during the period of

Figure 8 (facing). Ultrastructure of an *aip3*Δ strain. Strain DBY6939 (*aip3*-Δ1/*aip3*-Δ1) was prepared for immunoelectron microscopy with antiactin antibodies as described in MATERIALS AND METHODS.

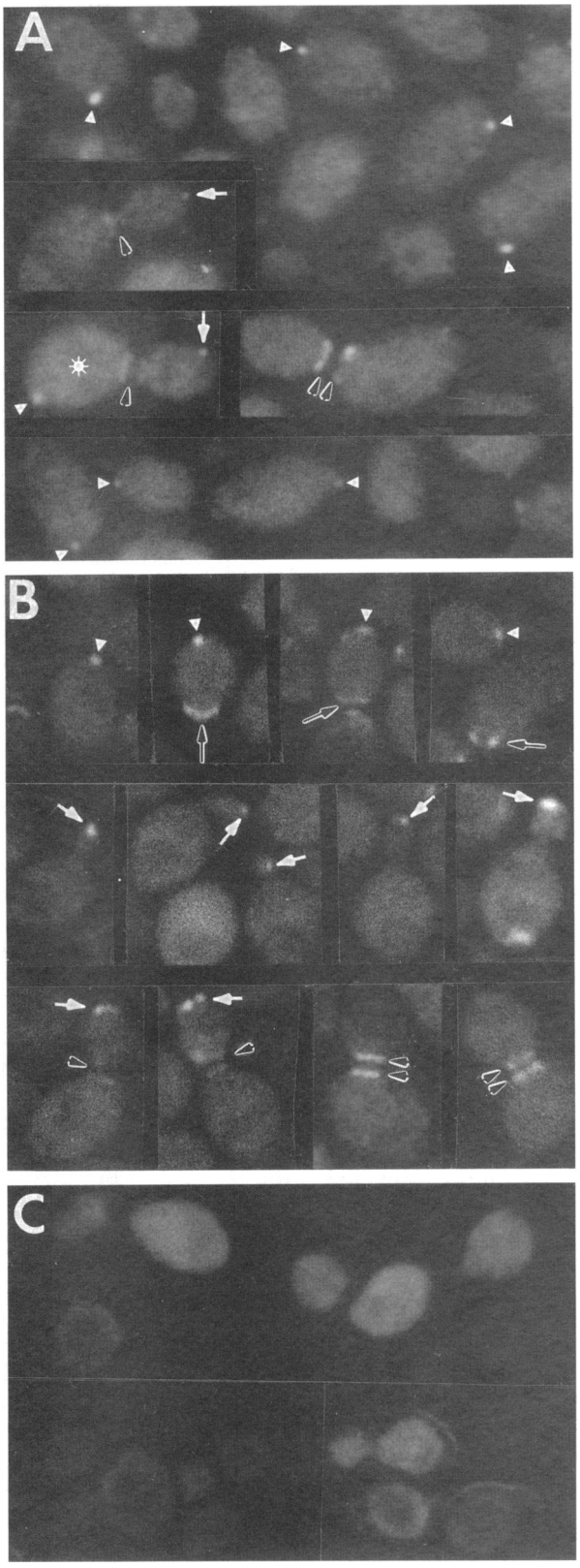

Figure 10.

observation, although their daughters both proceeded to form buds. Second, it was not possible to keep all parts of a field in focus at all times; thus, the initial appearance (or final disappearance) of a bud or a patch of GFP-Aip3p fluorescence could be missed if the relevant part of the field were out of focus at the time. For these reasons, our observations on the time intervals separating different events should be taken as rough estimates only. Finally, although the abrupt change in cell orientation makes cell separation a conspicuous event in the video records (see Figure 12, frames 18–26 for one cell and frames 26–34 for a second cell), we do not know the precise timing of this event relative to that of cytokinesis (the separation of mother and daughter cytoplasms by discrete plasma membranes). However, previous observations suggest that there is likely to be a lag of ~10 min between these events (Hartwell, 1971; Pringle and Mor, 1975).

Despite these caveats, the video records (Figure 12 presents frames from one typical series) provided striking confirmation of the conclusions derived from the static images and also revealed several additional features of the Aip3p localization patterns. First, the time-lapse observations provided unequivocal evidence that the bright patches of GFP-Aip3p fluorescence seen on unbudded cells represent the sites of subsequent bud emergence. In both mother and daughter cells (three daughter cells can be followed in Figure 12), the GFP-Aip3p patch was first seen at the presumptive budding site a considerable time before bud emergence (mean of approximately 24 min for 11 clear records, five of mother cells and six of daughter cells). In the daughter cells, the patch of GFP-Aip3p always appeared well after cell separation (mean of approximately 23 min for the six records), whereas for the mother cells, the patch of GFP-Aip3p always appeared significantly before cell separation (mean of approximately 10 min for the five records). Reproducibly, the signal at the presumptive bud site first appeared as a broad patch that then coalesced into a smaller more intense patch before bud emergence (Figure 12). The video records also showed clearly that small patches of GFP-Aip3p signal remained visible in

Figure 10. Localization of Aip3p by immunofluorescence with purified anti-Aip3p antibodies. White arrowheads indicate staining at presumptive bud sites or sites of very small buds; white arrows indicate staining at or near the tips of growing buds; single black arrowheads indicate faint staining at mother-bud necks of cells that also have patches of staining near the tips of their buds; double black arrowheads indicate brighter staining at the mother-bud necks of cells without patches of staining in their buds; black arrows indicate staining at recent division sites. * marks a cell referred to in the text. (A) Wild-type diploid strain YEF473. (B) Strain YEF473 harboring *AIP3* plasmid YEp352/H3.3. (C) *aip3-Δ3/aip3-Δ3* diploid strain YJZ358 (stained and photographed under conditions identical to those used for A and B). Cells were grown in YM-P medium (strains without plasmid) or in SC-Ura (strain with plasmid).

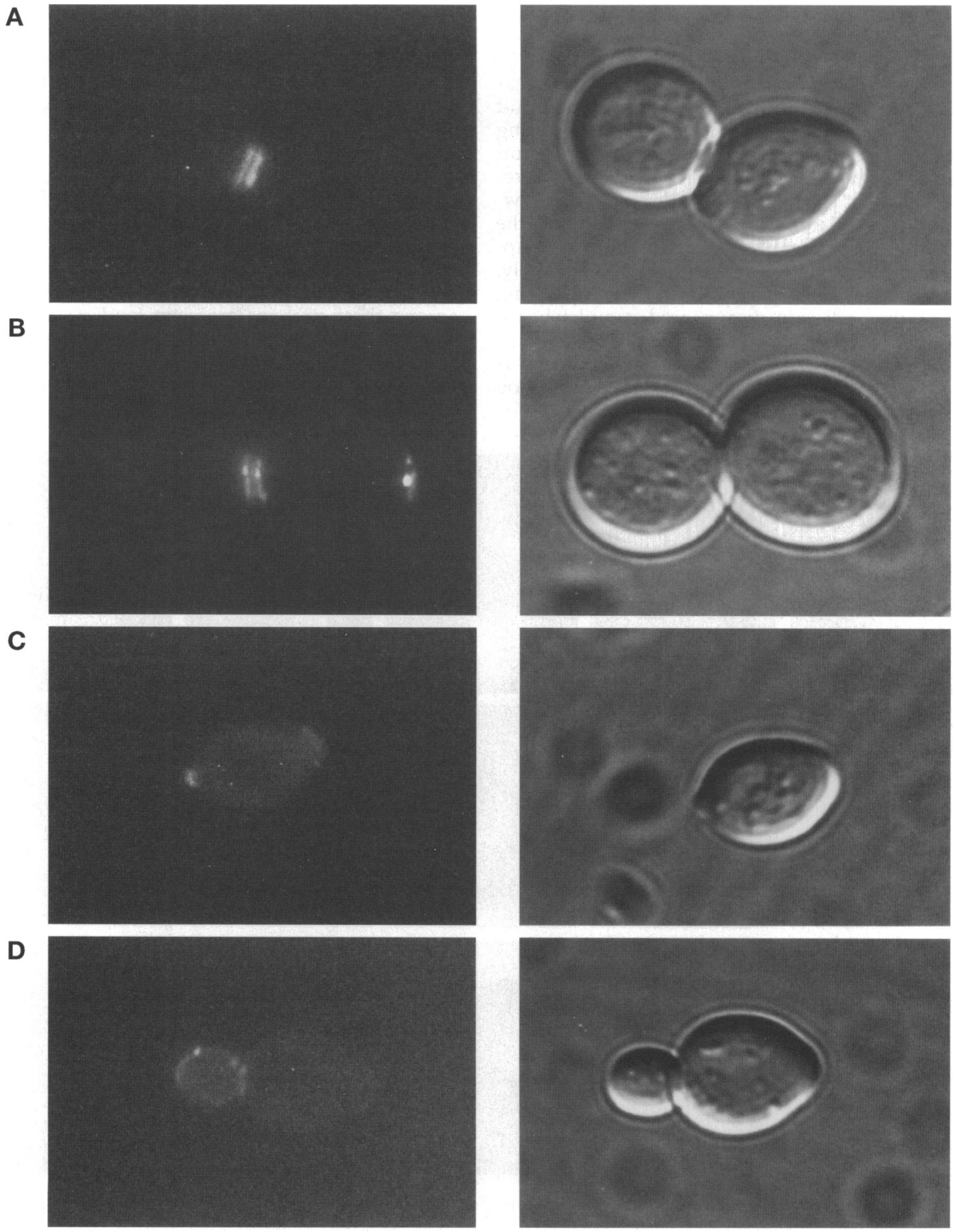

Figure 11. Localization of GFP-Aip3p through the yeast cell cycle. The low copy number plasmid pRB2190 expressing a GFP-Aip3p fusion protein was introduced into wild-type diploid strain DBY6525 and representative cells from an exponentially growing culture were visualized by fluorescence (left) and DIC (right) microscopy.

growing buds (predominantly, although not exclusively, near their tips) throughout most of the period of bud growth, disappearing only approximately 20 min prior to cell separation. In addition, it was clear that GFP-Aip3p was detectable at the mother-bud neck, as an apparent single ring, quite early during bud growth, within approximately 20 min after bud emergence (Figure 12). The GFP-Aip3p signal remained visible at the neck until cell separation; however, during the latter stages of the cell cycle, the signal became considerably brighter and began to appear as a double rather than a single ring. Remarkably, at (or just before) cell separation, the GFP-Aip3p ring on the mother cell side disappeared completely (or almost completely), whereas that on the daughter side remained strong, so that after cell separation there was a conspicous GFP-Aip3p signal marking the division site on the daughter cell but not on the mother cell (Figure 12). The ring of GFP-Aip3p at the daughter cells' division sites then began to disappear approximately coincident with the formation of patches of GFP-Aip3p at the new presumptive bud site (Figure 12).

Apparent Independence of Aip3p Localization from Actin and the Septins

Aip3p is one of a growing number of proteins that are known to localize to the presumptive bud site, to the bud tip, and/or to the mother-bud neck. Prominent among these proteins are actin (and associated proteins) and the septin proteins of the neck filaments (see INTRODUCTION). Actin and the septins appear to localize independently to the presumptive bud site

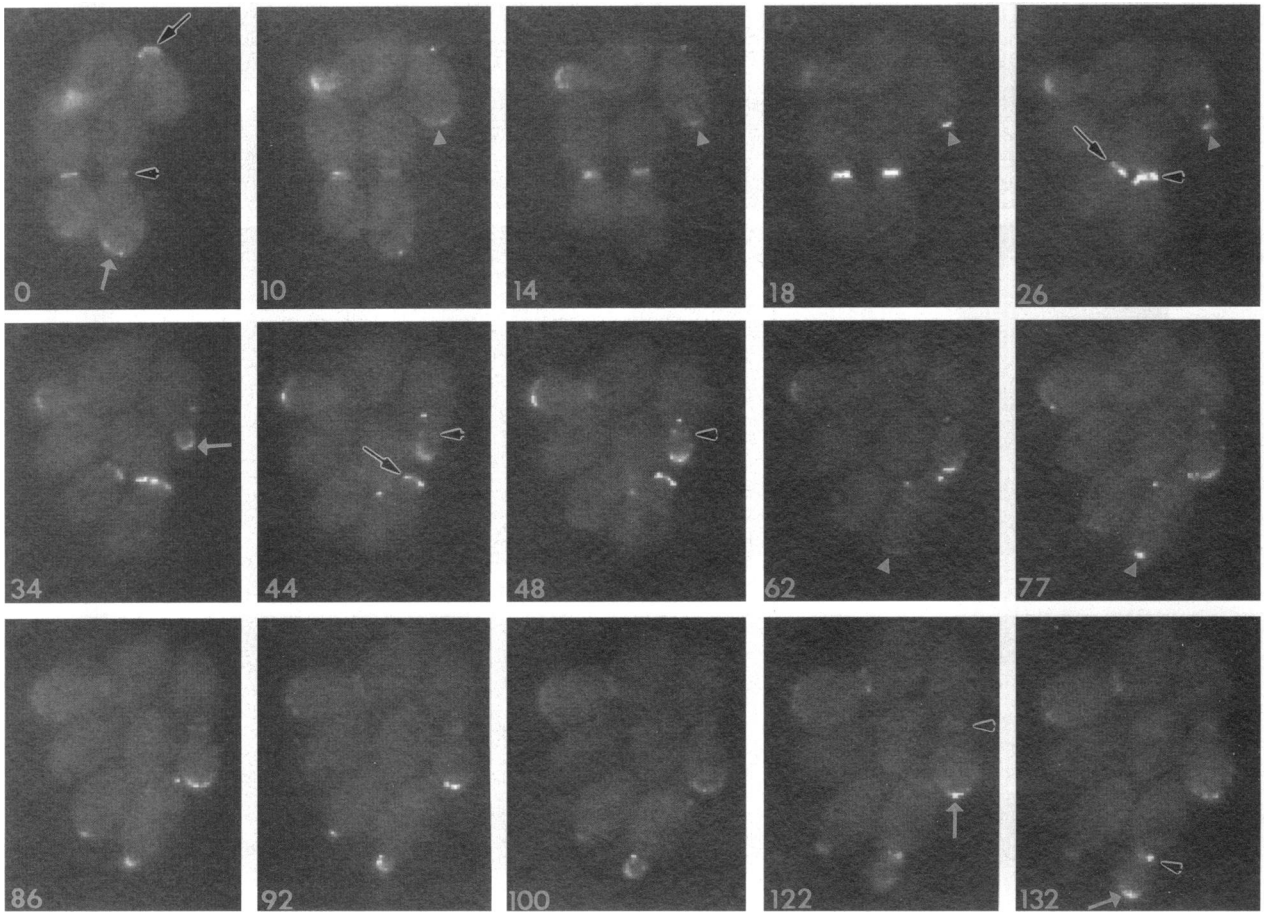

Figure 12. Time-lapse analysis of Aip3p localization. Wild-type diploid strain YEF473 harboring the GFP-*AIP3* plasmid pRB2190 was examined by time-lapse video microscopy as described in MATERIALS AND METHODS. Numbers indicate the time in minutes since the beginning of observation. White arrowheads indicate GFP-Aip3p signal at two incipient bud sites. White arrows indicate GFP-Aip3p signal at the tips of representative growing buds. Black arrowheads indicate GFP-Aip3p signal at representative mother-bud necks. An apparent double ring of staining was found at the mother-bud neck prior to cytokinesis in all cells examined, but the double rings are not well resolved in the printed video images (compare, however, Figures 10 and 11). Black arrows mark residual GFP-Aip3p signal at the division sites (birth scars) on daughter cells (identified as such by their smaller sizes and/or tip fluorescence at earlier points in the time-lapse series).

(Adams and Pringle, 1984; Ayscough *et al.*, 1997; Kim, Haarer, and Pringle, unpublished results) and then to provide the structural basis for the localization of a variety of other proteins to this site and (at least in the case of the septins) to the mother-bud neck (Chant *et al.*, 1995; Sanders and Herskowitz, 1996; Ayscough *et al.*, 1997; DeMarini and Pringle, unpublished results). Thus, it was important to ask whether the localization of Aip3p was dependent on actin, on the septins, or both. (The viability of the *aip3*Δ strains and the actin localization data described above made clear that both actin and the septins could localize at least approximately normally in the absence of Aip3p.) We performed several types of experiments to address these issues.

First, we examined more closely the relative timing of localization of the proteins of interest to the presumptive bud site. Actin and the septins both appear at this site ~15 min before bud emergence in rapidly growing unperturbed cultures (Kilmartin and Adams, 1984; Kim *et al.*, 1991; Snyder *et al.*, 1991; Ford and Pringle, 1991). From the Aip3p localization data described above, it seemed possible that Aip3p localized to the presumptive bud site earlier than this, which would eliminate the possibility that this aspect of Aip3p localization was dependent on actin or the septins. However, when we examined cells expressing GFP-Aip3p (strain YEF473 harboring plasmid pRB2190) that had also been fixed and stained with rhodamine-phalloidin to visualize actin, we found that most unbudded cells (>90%) showed either both proteins or neither protein at the presumptive bud site, suggesting that Aip3p and actin arrive at this site essentially simultaneously. Although we did observe a few cells that appeared to have Aip3p but not actin localized to a presumptive bud site (and vice versa), the inconsistent visualization of the two proteins in these double-label experiments means that this observation is not a strong argument for independence of localization.

In the same experiments, we examined more closely the timing of localization to the mother-bud neck. The septins are present at the neck throughout the period of bud growth (Ford and Pringle, 1991; Kim *et al.*, 1991), but actin becomes concentrated at the neck only very late in the cell cycle, after the chromosomes are fully separated and just before cell division (Adams and Pringle, 1984; Kilmartin and Adams, 1984; Lew and Reed, 1993; our unpublished results). Although it was clear from the Aip3p localization data described above that the initial localization of Aip3p to the neck occurred well before actin becomes concentrated there, it seemed possible that the transition in the Aip3p signal from a weak (and apparently single) ring to a strong (and apparently double) ring was coincident with, and thus possibly dependent on, the concentration of actin at the neck. However, in the double-label experiments, it seemed clear that the transition in the Aip3p signal significantly preceded the localization of actin to the neck. When cells were identified that had a strong double ring of GFP-Aip3p at the neck, at least half did not have a detectable concentration of actin at the neck and/or still had a single (or partially separated) mass of DNA as detected by bisbenzimide staining. In contrast, when cells were identified that had a detectable concentration of actin at the neck, essentially all of them had a strong double ring of GFP-Aip3p at the neck and two well-separated masses of DNA.

To explore these issues further, we took advantage of the observation that shifting yeast cells into conditions of high osmolarity causes, within 1 min, a transient loss of actin cables and a complete depolarization of actin cortical patches (Chowdhury *et al.*, 1992). We shifted an exponentially growing culture of strain DBY6525 harboring plasmid pRB2190 into medium containing 1 M NaCl and examined the localization of GFP-Aip3p at times from 5 min to 2 h after the shift. At no time was the pattern of GFP-Aip3p localization affected in the mother-bud neck, the bud cortex, or the presumptive bud sites on unbudded cells (about 200 cells counted at each time point). To confirm that these conditions indeed depolarized the actin cytoskeleton, we also fixed an aliquot of cells 15 min after the shift, stained F-actin with rhodamine-phalloidin, and simultaneously visualized GFP-Aip3p fluorescence. Despite a seemingly complete loss of actin cytoskeleton polarity, GFP-Aip3p localization was apparently unperturbed, supporting the hypothesis that the actin cytoskeleton is not responsible for Aip3p localization.

To explore the possible dependence of Aip3p localization upon the septins, we used a temperature-sensitive *cdc12–6* strain. Shift of such a strain from permissive to restrictive temperature results in a very rapid loss of localization to the mother-bud neck both of all of the septins (Ford and Pringle, 1991; Kim *et al.*, 1991) and of associated proteins such as Bud3p and Bud4p (Chant *et al.*, 1995; Sanders and Herskowitz, 1996). When exponentially growing cells of strain YJZ383 harboring plasmid pRB2190 were shifted from permissive (18°C) to restrictive (37°C) temperature, septin localization was lost in <10 min (Figure 13, K and L), as expected. However, GFP-Aip3p was still detectable 30 min after temperature shift at presumptive bud sites (Figure 13, A and B), in patches near the tips of buds (Figure 13, C and D), and at mother-bud necks (Figure 13, E–H). Even 90 min after temperature shift, GFP-Aip3p was still detectable at mother-bud necks (our unpublished observations) and at incipient buds (Figure 13, I and J). Thus, it appears that Aip3p localization both to incipient bud sites and to mother-bud necks is not dependent on the septins.

DISCUSSION

The *AIP3/BUD6* gene was identified by two independent approaches, one designed to find genes encoding actin-interacting proteins (Amberg *et al.*, 1995a) and the other designed to identify genes involved in the bipolar budding pattern (Zahner *et al.*, 1996). The observation that mutations in an actin-interacting protein affect the bipolar, but not the axial, budding pattern is consistent with other recent observations. In particular, mutations in actin itself and in a variety of other known or suspected actin-interacting proteins have also been reported to affect bipolar but not axial budding (Bauer *et al.*, 1993; Drubin *et al.*, 1993; Durrens *et al.*, 1995; Sivadon *et al.*, 1995; Yang *et al.*, 1997). In contrast, mutations in the septin proteins of the neck filaments have been shown to affect the axial budding pattern (Flescher *et al.*, 1993; Chant *et al.*, 1995), apparently because the septins are essential for localization of components (including Bud3p and Bud4p) of the transient positional signal upon which axial budding

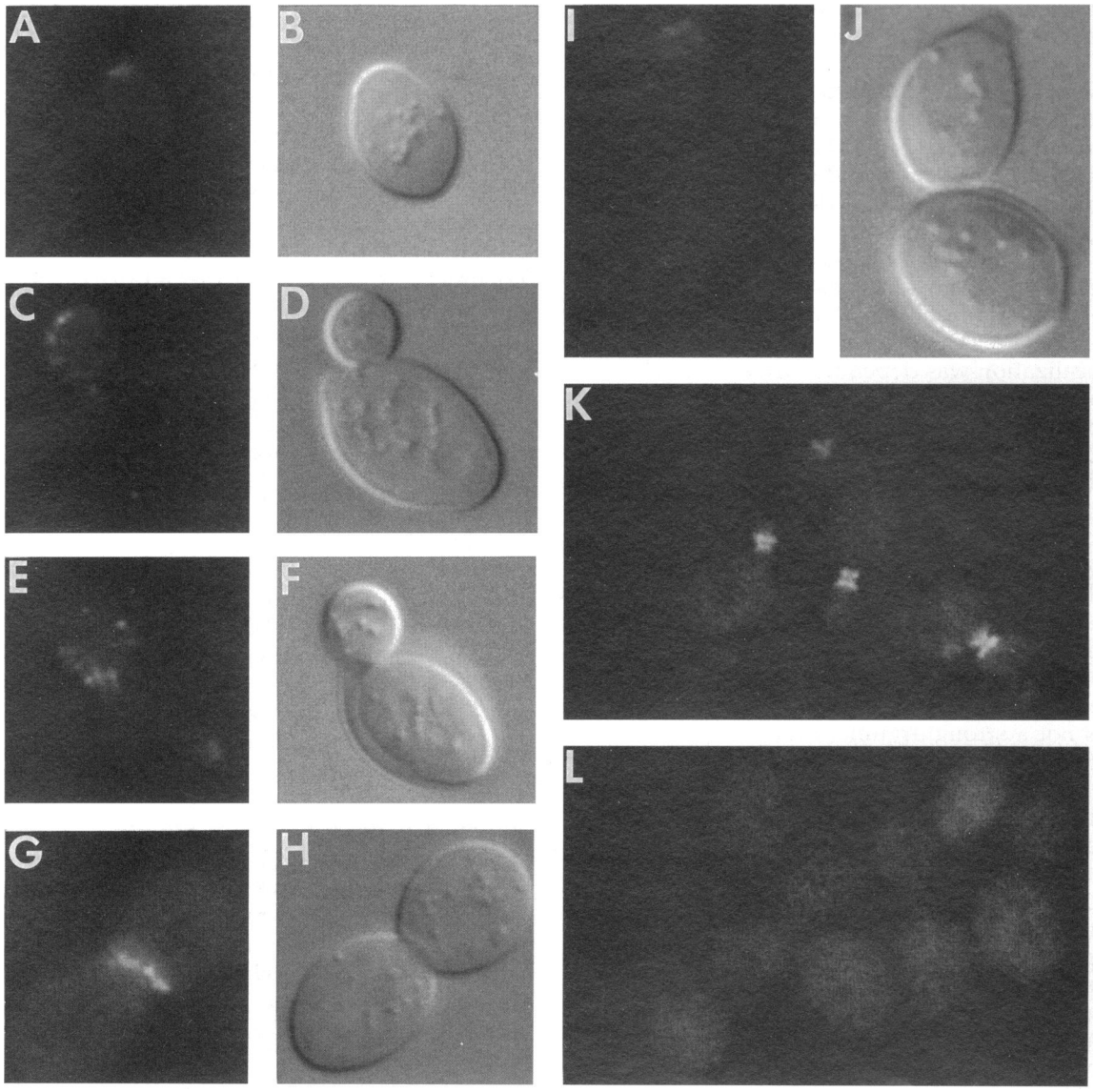

Figure 13. Persistence of Aip3p localization after septin disassembly in a temperature-sensitive septin mutant. Strain YJZ383 (*cdc12–6/cdc12–6*) containing plasmid pRB2190 was grown to exponential phase in SC-Ura medium at 18°C (permissive temperature) and then shifted to YM-P medium at 37°C (restrictive temperature). (A–J) Cells collected 30 (A–H) or 90 (I and J) min after the temperature shift were examined by fluorescence microscopy to visualize GFP-Aip3p (A, C, E, G, and I) or by DIC microscopy to visualize the cell outlines (B, D, F, H, and J). (K and L) Cells collected at the time of the temperature shift (K) or after 10 min at 37°C (L) were visualized by anti-Cdc11p immunofluorescence.

depends (Chant *et al.*, 1995; Chant and Pringle, 1995; Sanders and Herskowitz, 1996). Bipolar budding appears to depend on persistent or permanent positional signals that mark the distal pole of the daughter cell and the division site on both daughter and mother cells (Chant and Pringle, 1995; Pringle *et al.*, 1995; Zahner *et al.*, 1996). Thus, a plausible interpretation of the effects of mutations in actin and actin-associated proteins upon bipolar budding is that the actin cytoskeleton plays a role in the placement of the bipolar-specific positional signals.

In this regard, the details of the defect in bipolar budding produced by mutations affecting the actin cytoskeleton are of considerable interest. In all cases that have been examined (the original *bud6–1* mutation [Zahner *et al.*, 1996], the *aip3*Δ mutations characterized herein, *act1* mutations (Yang *et al.*, 1997), and mutations in several other actin-associated proteins [Yang *et al.*, 1997]), the mutant daughter cells appear to position their first bud sites almost normally at the distal pole. [The reduced fidelity of *bud6/aip3* mutants in using the very tip of the distal pole is a potentially revealing anomaly; see Zahner *et al.* (1996) for discussion of one possible interpretation. It is also possible that this is simply a rather nonspecific effect of the partial loss of cell polarization in the *aip3* mutants.] Subsequent bud sites then seem to be positioned essentially at random. The simplest interpretation of these observations is that the actin cytoskeleton is involved in placement of the bipolar positional signal at the division site on both mother and daughter cells but not in placement of the signal at the distal pole of the daughter cell. Thus, a newborn daughter cell would be able to position its first bud at the distal pole, but it would then have no other bipolar positional signals that could be recognized in subsequent cell cycles, so that its second and subsequent buds would be positioned randomly.

These considerations lead us to suggest modified versions of the models developed previously (Chant and Pringle, 1995) to account for the placement of the bipolar positional signals. In both of the modified models (Figure 14), the distal pole signal is placed at the presumptive bud site prior to bud emergence in an actin-independent manner. This is plausible, because the localization of a number of other proteins (such as the septins and Aip3p itself) to the presumptive bud site is known to be independent of actin (Kim, Haarer, and Pringle, unpublished observations; Ayscough *et al.*, 1997). This signal then simply remains in place as the bud grows around it, and thus successfully marks the distal pole of the daughter cell. In contrast, the division site signal would be positioned in an actin-dependent manner. This might occur prior to bud emergence (Figure 14, model B), a possibility rendered plausible by the observation that a variety of known proteins do localize to the presumptive bud site in an actin-dependent manner (Ayscough *et al.*, 1997). On this model, the signal would remain at the mother-bud neck during bud growth and partition between mother and daughter cells at division. It should be noted that in this model, the distal pole and division site signals would presumably need to involve different molecules. An alternative model, which we prefer, is that the division site signal only becomes localized late in the cell cycle when the actin cytoskeleton reorients toward the mother-bud neck in preparation for division (Figure 14, model A). Note that in this model, the distal pole and division site signals might involve either the same molecules, positioned at different times and by different mechanisms, or different molecules. If Aip3p were localized only to the presumptive bud site and bud tip or only to the mother-bud neck, its localization would have helped to discrimi-

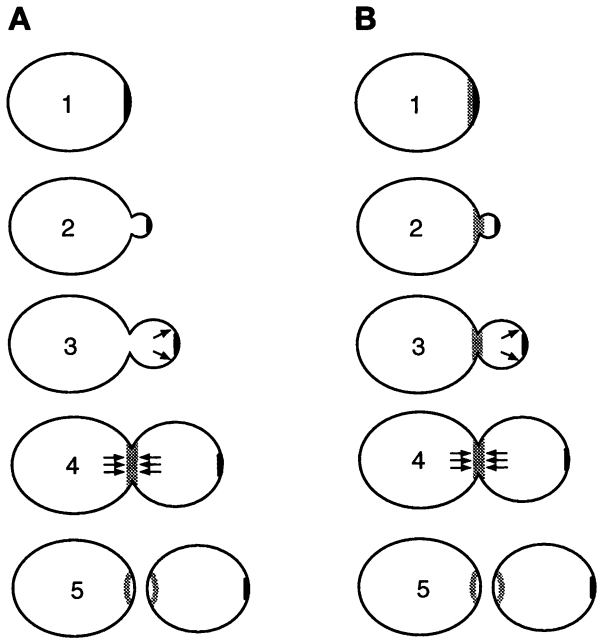

Figure 14. Models to explain the localization of the positional signals for bipolar budding. These models are modified from those developed previously (Chant and Pringle, 1995) to incorporate the evidence (see text) that the positioning of the distal pole signal (solid area) is actin independent but the positioning of the division site signal (shaded area) is actin dependent. (A) The distal pole signal is proposed to arrive at the presumptive bud site prior to bud emergence (cell 1) and to remain at the bud tip as the bud grows and cell division occurs (cells 2–5). In contrast, the division site signal is proposed to arrive at the mother-bud neck only late in the cell cycle when actin becomes concentrated there (cell 4) and to partition between mother and daughter cells at division (cell 5). (B) Both signals are proposed to arrive at the presumptive bud site prior to bud emergence (cell 1), but by different mechanisms, and to segregate at bud emergence (cell 2). The distal pole signal remains at the tip of the bud until cell division (cells 3–5), and the division site signal remains at the mother-bud neck as the bud grows (cells 3 and 4) and partitions at cell division (cell 5). In both models, small arrows indicate zones of localized cell surface growth.

nate between these models. Because Aip3p in fact localizes to both of the possible sites of action, discrimination between these models (or the rejection of both!) must await the identification and localization of authentic components of the division site signal. As mutations in *BUD9* lead to budding exclusively at the distal pole (Zahner *et al.*, 1996), its product is a good candidate for such a component.

Although the effect of *aip3* mutations on budding pattern is specific to **a**/α cells, Aip3p appears to be expressed and localized identically also in **a** and α cells, suggesting that its roles are not limited to bipolar bud-site selection. Indeed, the loss of Aip3p produces a variety of other phenotypes that are evident (to a greater or lesser extent) regardless of cell type and suggest that Aip3p has more general (albeit nonessential) roles in the organization and function of the actin cytoskeleton. Indeed, deletion of *AIP3* leads to a demonstrable depolarization of the actin cytoskeleton. This depolarization is not absolute: the *aip3*Δ cells are capable of forming buds, and many small budded cells appear to have polarized cytoskeletons. However, this polarity appears to be lost as the bud enlarges, and abnormal actin organization is also observed in the neck regions of cells preparing to divide. Presumably, the loss of actin cytoskeletal polarity results in the observed defects in polarization of the secretory pathway and in periods of isotropic growth that result in the formation of cells that are larger and rounder than normal. It is also likely that the broader necks and large, sometimes abnormal septa are secondary to defects in actin organization at the time of bud emergence (and initial organization of the neck), cytokinesis, or both.

In addition to their morphological abnormalities, the *aip3*Δ cells grow more slowly than control strains, although the severity of this phenotype varies with the strain background. This reduction in growth rate could be due, at least in part, to the inefficiencies that result from a loss of cell polarity, such as the division of growth potential between the mother and the bud (as opposed to directing all growth to the bud). However, the growth rate deficiency may also reflect defects in the nuclear cycle and/or in its coordination with other cell cycle events. We have observed that the *aip3*-Δ*1* and *aip3*-Δ*2* strains accumulate multinuclear cells, possibly as a result of poor nuclear positioning at karyokinesis. This is a phenotype common to many actin mutants (Drubin *et al.*, 1993) and could result from an inability of the cytoplasmic microtubules to find and/or attach to the bud cortex.

In addition, we have found that populations of the *aip3*-Δ*1* and *aip3*-Δ*2* strains contain about twice as many cells as normal in later stages of mitosis, indicating an arrest or delay late in the cell cycle. It is possible that the nuclear cycle may sense the poor preparation for cytokinesis in the neck region. The idea of coordination between the nuclear and cytoplasmic cycles is not unprecedented. Recently, a checkpoint coordinating bud emergence and nuclear division has been described; when bud emergence was inhibited, nuclear division was delayed (Lew and Reed, 1995). The only mutants in *S. cerevisiae* with clear defects in cytokinesis are those defective in the septins Cdc3p, Cdc10p, Cdc11p, and Cdc12p. Unlike the *aip3*Δ strains, the septin mutants display a complete failure of cytokinesis but no obvious defect in nuclear division or bud formation, so that multinuclear multibudded cells are formed (Hartwell, 1971; Adams and Pringle, 1984). This phenotype argues against coordination between nuclear and cytoplasmic division late in the cell cycle, unless the septins themselves form part of the checkpoint signaling mechanism.

An additional argument that the functions of Aip3p involve its interaction with actin comes from the observation that certain conditional alleles of *ACT1* have phenotypes very similar to that of an *AIP3* deletion. *act1–124* and *act1–133* cells have septation defects, and *act1–120* and *act1–119* cells have wide bud necks (Drubin *et al.*, 1993). In addition, these *act1* mutants also produce multinuclear cells and have cytoskeletons that are disorganized in ways similar to that of the *aip3*Δ strains; *act1–133* cells also are often abnormally large (Drubin *et al.*, 1993). These same *act1* alleles are the ones that affect the actin-Aip3p interaction. Thus, the defects seen in these actin mutants may all result from the inability of Aip3p to interact with actin.

If Aip3p functions by modulating the organization of the actin cytoskeleton and/or certain actin functions are mediated by Aip3p as an effector, it is clearly important to determine how Aip3p and actin influence each other's localization and behavior. In this regard, the available data are tantalizing. The localization of Aip3p and actin are similar but not identical: Both proteins localize to presumptive bud sites and the tips of small buds, but Aip3p appears to form a smooth patch whereas actin typically appears as a ring or cluster of smaller patches. Both proteins are present in patches that are concentrated near the tips of small and medium-sized buds, but it does not appear that the Aip3p and actin patches perfectly coincide. Both proteins localize to the mother-bud necks of cells with larger buds, but both the timing and the details of the localization patterns differ. Finally, both proteins are present at recent division sites, but Aip3p is present predominantly or exclusively on the daughter cell, whereas actin is present on both mother and daughter cells. Moreover, the localization of Aip3p does not appear to depend on actin, and the organization of the actin cytoskeleton is perturbed, but not completely disrupted, in the absence of Aip3p. The two-hybrid data suggest that Aip3p binds to actin across the ATP

cleft on the front surface of the actin monomer, a region of the molecule that remains solvent exposed in the model of the actin filament (Holmes *et al.*, 1990). We therefore cannot determine whether Aip3p is a G- or F-actin-binding protein. If Aip3p is a G actin-binding protein, binding across the ATP cleft might alter ATP exchange and/or hydrolysis and, therefore, regulate filament assembly at sites of polarized cell growth. We favor the alternative model that Aip3p is an F-actin-binding protein that affects the organization of F-actin at sites of polarized growth and/or helps to stabilize the polarized organization of the actin cytoskeleton.

In addition to interacting with actin, the C-terminal third of Aip3p shows a two-hybrid interaction with a larger fragment of Aip3p. It is likely that this interaction is mediated by the predicted coiled-coil domains near the Aip3p C terminus, but it remains possible that the interaction is mediated by other parts of the protein. Clarifying the functional consequences both of this interaction and of the Aip3p-actin interaction will be critical to understanding the organization and function of Aip3p in the cell.

Finally, the localization of Aip3p to the mother-bud neck suggests that Aip3p function may also involve an interaction with the septins. However, at present there is no other evidence for such an interaction. Indeed, it is remarkable that Aip3p and the septins appear to localize to the neck independently of each other. Of the various proteins known to localize to the neck, Aip3p is, to our knowledge, the only one known to remain at the neck when the septins disassemble in a *cdc12–6* mutant.

ACKNOWLEDGMENTS

We thank Steve Elledge, Fred Winston, Phil Hieter, and Erfei Bi for strains and plasmids; Tim Doyle for constructing plasmid pRB2190; Ted Salmon and members of his laboratory for assistance with video micrography; Heidi Harkins for stimulating discussions and collaboration in the bipolar mutants project; Mark Johnston for providing chromosome XII sequence data in advance of its formal release; and Kathryn Ayscough, Shirley Yang, and David Drubin for providing information in advance of publication and for stimulating discussions. This research was supported by National Institutes of Health Grants GM-46888 and GM-46406 (to D.B.) and GM-31006 (to J.R.P.) and by the RJEG Trust. J.Z. was supported by National Institutes of Health Postdoctoral Fellowship GM-16478. D.C.A. was a Smith Kline Beecham Pharmaceuticals Fellow of the Life Sciences Research Foundation.

REFERENCES

Adams, A.E.M., Botstein, D., and Drubin, D.G. (1991). Requirement of yeast fimbrin for actin organization and morphogenesis in vivo. Nature *354*, 404–408.

Adams, A.E.M., and Pringle, J.R. (1984). Relationship of actin and tubulin distribution to bud growth in wild-type and morphogenetic-mutant *Saccharomyces cerevisiae*. J. Cell Biol. *98*, 934–945.

Altschul, S.F., Gish, W., Miller, W., Myers, E.W., and Lipman, D.J. (1990). Basic local alignment search tool. J. Mol. Biol. *215*, 403–410.

Amatruda, J.F., and Cooper, J.A. (1992). Purification, characterization, and immunofluorescence localization of *Saccharomyces cerevisiae* capping protein. J. Cell Biol. *117*, 1067–1076.

Amberg, D.C., Basart, E., and Botstein, D. (1995a). Defining protein interactions with yeast actin in vivo. Nat. Struct. Biol. *2*, 28–35.

Amberg, D.C., Botstein, D., and Beasley, E.M. (1995b). Precise gene disruption in *Saccharomyces cerevisiae* by double fusion polymerase chain reaction. Yeast *11*, 1275–1280.

Ausubel, F.M., Brent, R., Kingston, R.E., Moore, D.D., Seidman, J.G., Smith, J.A., and Struhl, K. (eds.) (1989). Current Protocols in Molecular Biology, New York: John Wiley & Sons.

Ayscough, K.R., Stryker, J., Pokala, N., Sanders, M., Crews, P., and Drubin, D.G. High rates of actin filament turnover in budding yeast and roles for actin in establishment and maintenance of cell polarity revealed using the actin inhibitor latrunculin-A. (1997). J. Cell Biol. (*in press*).

Baudin, A., Ozier-Kalogeropoulos, O., Denouel, A., Lacroute, F., and Cullin, C. (1993). A simple and efficient method for direct gene deletion in *Saccharomyces cerevisiae*. Nucleic Acids Res. *21*, 3329–3330.

Bauer, F., Urdaci, M., Aigle, M., and Crouzet, M. (1993). Alteration of a yeast SH3 protein leads to conditional viability with defects in cytoskeletal and budding patterns. Mol. Cell. Biol. *13*, 5070–5084.

Becker, D.M., and Guarente, L. (1991). High-efficiency transformation of yeast by electroporation. Methods Enzymol. *194*, 182–187.

Bénédetti, H., Raths, S., Crausaz, F., and Riezman, H. (1994). The *END3* gene encodes a protein that is required for the internalization step of endocytosis and for actin cytoskeleton organization in yeast. Mol. Biol. Cell *5*, 1023–1037.

Bi, E., and Pringle, J.R. (1996). *ZDS1* and *ZDS2*, genes whose products may regulate Cdc42p in *Saccharomyces cerevisiae*. Mol. Cell. Biol. *16*, 5264–5275.

Bilbe, G., *et al.* (1992). Restin: a novel intermediate filament-associated protein highly expressed in the Reed-Sternberg cells of Hodgkin's disease. EMBO J. *11*, 2103–2113.

Bretscher, A., Drees, B., Harsay, E., Schott, D., and Wang, T. (1994). What are the basic functions of microfilaments? Insights from studies in budding yeast. J. Cell Biol. *126*, 821–825.

Byers, B. (1981). Cytology of the yeast life cycle. In: The Molecular Biology of the Yeast *Saccharomyces*. Life Cycle and Inheritance, ed. J.N. Strathern, E.W. Jones, and J.R. Broach, Cold Spring Harbor, NY: Cold Spring Harbor Laboratory Press, 59–96.

Byers, B., and Goetsch, L. (1976a). A highly ordered ring of membrane-associated filaments in budding yeast. J. Cell Biol. *69*, 717–721.

Byers, B., and Goetsch, L. (1976b). Loss of the filamentous ring in cytokinesis-defective mutants of budding yeast. J. Cell Biol. *70*, 35A (Abstract).

Chalfie, M., Tu, Y., Euskirchen, G., Ward, W.W., and Prasher, D.C. (1994). Green fluorescent protein as a marker for gene expression. Science *263*, 802–805.

Chant, J., and Herskowitz, I. (1991). Genetic control of bud site selection in yeast by a set of gene products that constitute a morphogenetic pathway. Cell *65*, 1203–1212.

Chant, J., Mischke, M., Mitchell, M., Herskowitz, I., and Pringle, J.R. (1995). Role of Bud3p in producing the axial budding pattern of yeast. J. Cell Biol. *129*, 767–778.

Chant, J., and Pringle, J.R. (1995). Patterns of bud-site selection in the yeast *Saccharomyces cerevisiae*. J. Cell Biol. *129*, 751–765.

Chen, X., Sullivan, D.S., and Huffaker, T.C. (1994). Two yeast genes with similarity to TCP-1 are required for microtubule and actin function in vivo. Proc. Natl. Acad. Sci. USA *91*, 9111–9115.

Chowdhury, S., Smith, K.W., and Gustin, M. (1992). Osmotic stress and the yeast cytoskeleton: phenotype-specific suppression of an actin mutation. J. Cell Biol. *118*, 561–571.

Doyle, T., and Botstein, D. (1996). Movement of yeast cortical actin cytoskeleton visualized in vivo. Proc. Natl. Acad. Sci. USA *93*, 3886–3891.

Drees, B., Brown, C., Barrell, B.G., and Bretscher, A. (1995). Tropomyosin is essential in yeast, yet the *TPM1* and *TPM2* products perform distinct functions. J. Cell Biol. *128*, 383–392.

Drubin, D.G., Jones, H.D., and Wertman, K.F. (1993). Actin structure and function: roles in mitochondrial organization and morphogenesis in budding yeast and identification of the phalloidin-binding site. Mol. Biol. Cell *4*, 1277–1294.

Drubin, D.G., and Nelson, W.J. (1996). Origins of cell polarity. Cell *84*, 335–344.

Durrens, P., Revardel, E., Bonneu, M., and Aigle, M. (1995). Evidence for a branched pathway in the polarized cell division of *Saccharomyces cerevisiae*. Curr. Genet. *27*, 213–216.

Feinberg, A.P., and Vogelstein, B. (1983). A technique for radiolabeling DNA restriction endonuclease fragments to high specific activity. Anal. Biochem. *132*, 6–13.

Fields, S., and Song, O. (1989). A novel genetic system to detect protein-protein interactions. Nature *340*, 245–246.

Fishkind, D.J., and Wang, Y. (1995). New horizons for cytokinesis. Curr. Opin. Cell Biol. *7*, 23–31.

Flescher, E.G., Madden, K., and Snyder, M. (1993). Components required for cytokinesis are important for bud site selection in yeast. J. Cell Biol. *122*, 373–386.

Ford, S.K., and Pringle, J.R. (1991). Cellular morphogenesis in the *Saccharomyces cerevisiae* cell cycle: localization of the *CDC11* gene product and the timing of events at the budding site. Dev. Genet. *12*, 281–292.

Gietz, R.D., and Sugino, A. (1988). New yeast-*Escherichia coli* shuttle vectors constructed with in vitro mutagenized yeast genes lacking six-base pair restriction sites. Gene *74*, 527–534.

Goodson, H.V., Anderson, B.L., Warrick, H.M., Pon, L.A., and Spudich, J.A. (1996). Synthetic lethality screen identifies a novel yeast myosin I gene (*MYO5*): myosin I proteins are required for polarization of the actin cytoskeleton. J. Cell Biol. *133*, 1277–1291.

Goodson, H.V., and Spudich, J.A. (1995). Identification and molecular characterization of a yeast myosin I. Cell Motil. Cytoskeleton *30*, 73–84.

Haarer, B.K., Petzold, A., Lillie, S.H., and Brown, S.S. (1994). Identification of *MYO4*, a second class V myosin gene in yeast. J. Cell Sci. *107*, 1055–1064.

Harlow, E., and Lane, D. (1988). Antibodies: A Laboratory Manual, Cold Spring Harbor, NY: Cold Spring Harbor Laboratory Press.

Hartwell, L.H. (1971). Genetic control of the cell division cycle in yeast. IV. Genes controlling bud emergence and cytokinesis. Exp. Cell Res. *69*, 265–276.

Hill, J.E., Myers, A.M., Koerner, T.J., and Tzagoloff, A. (1986). Yeast/*E. coli* shuttle vectors with multiple unique restriction sites. Yeast *2*, 163–167.

Holmes, K.C., Popp, D., Gebhard, W., and Kabsch, W. (1990). Atomic model of the actin filament. Nature *347*, 44–49.

Holtzman, D.A., Wertman, K.F., and Drubin, D.G. (1994). Mapping actin surfaces required for functional interactions in vivo. J. Cell Biol. *126*, 423–432.

Honts, J.E., Sandrock, T.S., Brower, S.M., O'Dell, J.L., and Adams, A.E.M. (1994). Actin mutations that show suppression with fimbrin mutations identify a likely fimbrin-binding site on actin. J. Cell Biol. *126*, 413–422.

Iida, K., Moriyama, K., Matsumoto, S., Kawasaki, H., Nishida, E., and Yahara, I. (1993). Isolation of a yeast essential gene, *COF1*, that encodes a homologue of mammalian cofilin, a low-M(r) actin-binding and depolymerizing protein. Gene *124*, 115–120.

Ito, H., Fukuda, Y., Murata, K., and Kimura, A. (1983). Transformation of intact yeast cells treated with alkali cations. J. Bacteriol. *153*, 163–168.

Johnston, G.C., Prendergast, J.A., and Singer, R.A. (1991). The *Saccharomyces cerevisiae MYO2* gene encodes an essential myosin for vectorial transport of vesicles. J. Cell Biol. *113*, 539–551.

Jones, J.S., and Prakash, L. (1990). Yeast *Saccharomyces cerevisiae* selectable markers in pUC18 polylinkers. Yeast *6*, 363–366.

Kabsch, W., Mannherz, H.G., Suck, D., Pai, E.F., and Holmes, K.C. (1990). Atomic structure of the actin:DNase I complex. Nature *347*, 37–44.

Kilmartin, J.V, and Adams, A.E.M. (1984). Structural rearrangements of tubulin and actin during the cell cycle of the yeast *Saccharomyces*. J. Cell Biol. *98*, 922–933.

Kim, H.B., Haarer, B.K., and Pringle, J.R. (1991). Cellular morphogenesis in the *Saccharomyces cerevisiae* cell cycle: localization of the *CDC3* gene product and the timing of events at the budding site. J. Cell Biol. *112*, 535–544.

Kölling, R., Nguyen, T., Chen, E.Y., and Botstein, D. (1993). A new yeast gene with a myosin-like heptad repeat structure. Mol. Gen. Genet. *237*, 359–369.

Kübler, E., and Riezman, H. (1993). Actin and fimbrin are required for the internalization step of endocytosis in yeast. EMBO J. *12*, 2855–2862.

Laemmli, U.K. (1970). Cleavage of structural proteins during the assembly of the head of bacteriophage T4. Nature *227*, 680–685.

Lew, D.J., and Reed, S.I. (1993). Morphogenesis in the yeast cell cycle: regulation by Cdc28 and cyclins. J. Cell Biol. *120*, 1305–1320.

Lew, D.J., and Reed, S.I. (1995). A cell cycle checkpoint monitors cell morphogenesis in budding yeast. J. Cell Biol. *129*, 739–749.

Lillie, S.H., and Pringle, J.R. (1980). Reserve carbohydrate metabolism in *Saccharomyces cerevisiae*: responses to nutrient limitation. J. Bacteriol. *143*, 1384–1394.

Liu, H., and Bretscher, A. (1989). Disruption of the single tropomyosin gene in yeast results in the disappearance of actin cables from the cytoskeleton. Cell *57*, 233–242.

Longtine, M.S., DeMarini, D.J., Valencik, M.L., Al-Awar, O.S., Fares, H., De Virgilio, C., and Pringle, J.R. (1996). The septins: roles in cytokinesis and other processes. Curr. Opin. Cell Biol. *8*, 106–119.

Lupas, A., Van Dyke, M., and Stock, J. (1991). Predicting coiled coils from protein sequences. Science *252*, 1162–1164.

Magdolen, V., Oechsner, U., Müller, G., and Bandlow, W. (1988). The intron-containing gene for yeast profilin (*PFY*) encodes a vital function. Mol. Cell. Biol. *8*, 5108–5115.

Miklos, D., *et al.* (1994). Primary structure and function of a second essential member of the heterooligomeric TCP1 chaperonin complex of yeast, TCP1β. Proc. Natl. Acad. Sci. USA *91*, 2743–2747.

Moon, A.L., Janmey, P.A., Louie, K.A., and Drubin, D.G. (1993). Cofilin is an essential component of the yeast cortical cytoskeleton. J. Cell Biol. *120*, 421–435.

Mulholland, J., Preuss, D., Moon, A., Wong, A., Drubin, D., and Botstein, D. (1994). Ultrastructure of the yeast actin cytoskeleton and its association with the plasma membrane. J. Cell Biol. *125*, 381–391.

Novick, P., and Botstein, D. (1985). Phenotypic analysis of temperature-sensitive yeast actin mutants. Cell *40*, 405–416.

Preuss, D., Mulholland, J., Franzusoff, A., Segev, N., and Botstein, D. (1992). Characterization of the *Saccharomyces* Golgi complex through the cell cycle by immunoelectron microscopy. Mol. Biol. Cell *3*, 789–803.

Pringle, J.R., Bi, E., Harkins, H.A., Zahner, J.E., De Virgilio, C., Chant, J., Corrado, K., and Fares, H. (1995). Establishment of cell polarity in yeast. Cold Spring Harbor Symp. Quant. Biol. *60*, 729–744.

Pringle, J.R., and Hartwell, L.H. (1981). The *Saccharomyces cerevisiae* cell cycle. In: The Molecular Biology of the Yeast *Saccharomyces*. Life Cycle and Inheritance, ed. J.N. Strathern, E.W. Jones, and J.R. Broach, Cold Spring Harbor, NY: Cold Spring Harbor Laboratory Press, 97–142.

Pringle, J.R., and Mor, J.-R. (1975). Methods for monitoring the growth of yeast cultures and for dealing with the clumping problem. Methods Cell Biol. *11*, 131–168.

Pringle, J.R., Preston, R.A., Adams, A.E.M., Stearns, T., Drubin, D.G., Haarer, B.K., and Jones, E.W. (1989). Fluorescence microscopy methods for yeast. Methods Cell Biol. *31*, 357–435.

Riles, L., Dutchik, J.E., Baktha, A., McCauley, B.K., Thayer, E.C., Leckie, M.P., Braden, V.V., Depke, J.E., and Olson, M.V. (1993). Physical maps of the six smallest chromosomes of *Saccharomyces cerevisiae* at a resolution of 2.6 kilobase pairs. Genetics *134*, 81–150.

Rodriguez, J.R., and Paterson, B.M. (1990). Yeast myosin heavy chain mutant: Maintenance of the cell type specific budding pattern and the normal deposition of chitin and cell wall components requires an intact myosin heavy chain gene. Cell Motil. Cytoskeleton *17*, 301–308.

Rose, M.D., Winston, F., and Hieter, P. (1989). Methods in Yeast Genetics, Cold Spring Harbor, NY: Cold Spring Harbor Laboratory Press.

Sambrook, J., Fritsch, E.F., and Maniatis, T. (1989). Molecular Cloning: A Laboratory Manual, 2nd ed., Cold Spring Harbor, NY: Cold Spring Harbor Laboratory Press.

Sanders, S.L., and Herskowitz, I. (1996). J. Cell Biol. *134*, 413–427.

Schmidt, A., Heid, H.W., Schäfer, S., Nuber, U.A., Zimbelmann, R., and Franke, W.W. (1994). Desmosomes and cytoskeletal architecture in epithelial differentiation: cell type-specific plaque components and intermediate filament anchorage. Eur. J. Cell Biol. *65*, 229–245.

Sikorski, R.S., and Hieter, P. (1989). A system of shuttle vectors and yeast host strains designed for efficient manipulation of DNA in *Saccharomyces cerevisiae*. Genetics *122*, 19–27.

Sivadon, P., Bauer, F., Aigle, M., and Crouzet, M. (1995). Actin cytoskeleton and budding pattern are altered in the yeast *rvs161* mutant: the Rvs161 protein shares common domains with the brain protein amphiphysin. Mol. Gen. Genet. *246*, 485–495.

Snyder, M., Gehrung, S., and Page, B.D. (1991). Studies concerning the temporal and genetic control of cell polarity in *Saccharomyces cerevisiae*. J. Cell Biol. *114*, 515–532.

Sweeney, F.P., Pocklington, M.J., and Orr, E. (1991). The yeast type II myosin heavy chain: analysis of its predicted polypeptide sequence. J. Muscle Res. Cell Motil. *12*, 61–68.

Thorne, K.J.I., Thornley, M.J., Naisbett, P., and Glauert, A.M. (1975). The nature of the attachment of a regularly arranged surface protein to the outer membrane of an *Acinetobacter sp.* Biochim. Biophys. Acta *389*, 97–116.

Towbin, H., Staehelin, T., and Gordon, J. (1979). Electrophoretic transfer of proteins from polyacrylamide gels to nitrocellulose sheets: procedure and some applications. Proc. Natl. Acad. Sci. USA *76*, 4350–4354.

Ursic, D., and Culbertson, M.R. (1991). The yeast homolog to mouse *Tcp-1* affects microtubule-mediated processes. Mol. Cell. Biol. *11*, 2629–2640.

Vinh, D.B.-N., and Drubin, D.G. (1994). A yeast TCP-1-like protein is required for actin function in vivo. Proc. Natl. Acad. Sci. USA *91*, 9116–9120.

Waddle, J.A., Karpova, T.S., Waterston, R.H., and Cooper, J.A. (1996). Movement of cortical actin patches in yeast. J. Cell Biol. *132*, 861–870.

Welch, M.D., Holtzman, D.A., and Drubin, D.G. (1994). The yeast actin cytoskeleton. Curr. Opin. Cell Biol. *6*, 110–119.

Wertman, K.F., Drubin, D.G., and Botstein, D. (1992). Systematic mutational analysis of the yeast *ACT1* gene. Genetics *132*, 337–350.

Yang, S., Ayscough, K.R., and Drubin, D.G. (1997). A role for the actin cytoskeleton of *Saccharomyces cerevisiae* in bipolar bud-site selection. J. Cell Biol. *136*, 111–123.

Zahner, J.E., Harkins, H.A., and Pringle, J.R. (1996). Genetic analysis of the bipolar pattern of bud site selection in the yeast *Saccharomyces cerevisiae*. Mol. Cell. Biol. *16*, 1857–1870.-